Nde1 is a Biphasic Regulator of the Dynein Activation Pathway

Yuanchang Zhao[1,2], Sena Oten[2], Ahmet Yildiz[1,2,3*]

[1] Physics Department, University of California, Berkeley, CA, USA, 94709

[2] Department of Molecular and Cell Biology, University of California, Berkeley, CA, USA, 94709

[3] Biophysics Graduate Group, University of California, Berkeley, CA, USA, 94709

[*]Correspondence to: Ahmet Yildiz (yildiz@berkeley.edu)

Abstract

Cytoplasmic dynein is the primary motor that drives the motility and force generation functions towards the microtubule minus end. The activation of dynein motility requires its assembly with dynactin and a cargo adaptor. This process is facilitated by two dynein-associated factors, Lis1 and Nde1/Ndel1. Recent studies proposed that Lis1 rescues dynein from its autoinhibited conformation, but the physiological function of Nde1/Ndel1 remains elusive. Here, we investigated how human Nde1 and Lis1 regulate the assembly and subsequent motility of the mammalian dynein/dynactin complex using in vitro reconstitution and single molecule imaging. We found that Nde1 promotes the assembly of active dynein complexes by competing with the inhibitor of Lis1, PAFAH-α2, and recruiting Lis1 to dynein. However, excess Nde1 inhibits dynein, presumably by competing against dynactin to bind the dynein intermediate chain. The association of dynactin with dynein triggers Nde1 dissociation before the initiation of dynein motility. Our results provide a mechanistic explanation for how Nde1 and Lis1 synergistically activate the dynein transport machinery.

Introduction

Cytoplasmic dynein-1 (dynein hereafter) drives retrograde transport of a wide variety of intracellular cargos, including membranous organelles, vesicles, mRNA, and unfolded proteins. Dynein also plays essential roles in cell division, including nuclear envelope breakdown, focusing the mitotic spindle, and transporting spindle assembly checkpoint signals[1]. Mutations in dynein and its regulatory proteins have been linked to severe developmental and neurological disorders, including spinal muscular atrophy, motor neuron degeneration, ALS, and schizophrenia[2].

Dynein is composed of a homodimer of heavy chains and several intermediate, light-intermediate, and light chains associated with the heavy chain. Motility is driven by the C-terminal motor domain of the heavy chain, which contains a catalytic ring of six AAA subunits, a microtubule-binding domain, and other mechanical elements that drive minus-end directed motility[3]. Similar to kinesin[4], isolated dynein remains in an autoinhibited (phi) conformation through direct interactions between its two motor domains[5, 6]. Dynein motility is activated by its association with a multi-subunit complex, dynactin, and the coiled-coil domain of an activating adaptor that links the motor to its cellular cargo (DDA complex)[7-10].

The assembly, activation, and subsequent motility of the dynein transport machinery are highly regulated by accessory proteins, Lis1 and Nde1/Ndel1[11]. Lis1 is the only known protein that directly binds to the motor domain of dynein and is required for virtually all dynein functions in the cytoplasm of eukaryotic cells[11, 12]. Mutations in Lis1 have been shown to disrupt many dynein-driven processes in cells and heterozygous mutations to Lis1 cause the brain neurodevelopmental disease, lissencephaly[11]. Lis1 forms a homodimer through its N-terminal LisH domain[13, 14] and binds to the AAA+ ring and stalk of dynein through its β-propeller domains[15]. Recent in vitro studies proposed that Lis1 binding to the dynein motor domain is incompatible with self-interactions between the two motor domains in the phi conformation, thereby promoting the formation of DDA complexes[16-18]. After the initiation of transport, Lis1 is not required for processive motility and its dissociation from DDA has been reported to result in faster motility[16-19]. These results are compatible with studies of Lis1 in live cells[20-27] and provide a mechanistic explanation for why Lis is required for dynein-mediated transport.

Nde1 and Ndel1 are highly conserved proteins that play important roles in the dynein-driven transport of intracellular cargos and nuclear oscillations in developing neurons, as well as dynein-mediated functions in mitosis[28]. Nde1/Ndel1 contains an N-terminal coiled-coil domain that interacts with the dynein intermediate chain (DIC) and the β-propeller domain of Lis1, whereas the C-terminus is mostly disordered[29-32]. While Lis1 deletion is deleterious for most dynein-driven processes[22, 33], Nde1 or Ndel1 deletion results in relatively milder phenotypes[22, 34, 35], possibly due to overlapping functions of Nde1 and Ndel1. However, co-depletion of Nde1 and Ndel1, or Nde1/Ndel1 and Lis1 have been shown to severely impair retrograde transport[22, 34]. While the phenotype caused by Nde1 deletion in *Xenopus* egg extracts could be rescued by exogenous addition of purified Lis1, Lis1 deletion could not be rescued by Nde1 addition, demonstrating that Nde1 function is dependent on Lis1[36].

The mechanism by which Nde1/Ndel1 (Nde1 hereafter) regulates the dynein activation pathway together with Lis1 is not well understood. Studies in live cells suggested that Nde1's primary function is to tether Lis1 to dynein, increasing its apparent affinity for dynein[36-38]. Consistent with this model, the Nde1 mutant that cannot bind dynein failed to rescue a mitotic phenotype caused by Nde1 depletion[39]. Similarly, the expression of a dynein mutant that cannot adopt the phi conformation partially rescued defects in Nde1 depletion in filamentous fungi[40]. Nde1 overexpression rescues phenotypes caused by depletion, but not deletion, of Lis1[34, 41]. However, strong overexpression or the addition of excess Nde1 have been shown to cause a dominant negative effect on dynein driven processes in many organisms[21, 36, 42, 43], but how excess Nde1 disrupts dynein function remained unknown.

The tethering model has been challenged by several observations made in vivo and in vitro. Overexpression of Nde1 mutant that cannot bind Lis1 was sufficient to rescue mitotic phenotypes of Nde1 depletion in several cell types[39, 44]. In vitro studies showed that while Lis1 promotes the assembly of the DDA complex[16-18], Nde1 competes against the p150 subunit of dynactin to interact with the dynein intermediate chain[31, 45, 46]. Furthermore, Lis1 increases whereas Nde1 decreases the microtubule-binding affinity of isolated dynein[12, 30, 47, 48]. These observations indicate that Nde1's role in the dynein activation pathway is more complex than tethering Lis1 to dynein and may also involve Nde1-mediated regulation of dynein independent of Lis1. Consistent with the possibility that Nde1 and Lis1 have related but distinct roles in the dynein pathway, Nde1 and Lis1 mutations are linked to distinct neurodevelopmental diseases[38, 49].

Early in vitro studies have reported conflicting information on whether Nde1 enhances dynein activity or inhibits it[12, 30, 47]. These studies were performed before it was understood that dynein remains inactive in the absence of dynactin and an adaptor protein[5, 8, 9, 50]. To understand the role of Nde1 in the dynein activation pathway, we directly monitored the assembly and motility of the mammalian dynein-dynactin-BicDR1 (DDR) complex in the presence of human Lis1 and Ndel1 in vitro. We observed that Nde1 functions as a biphasic regulator of dynein. Lower concentrations of full-length or N-terminal coiled-coil of Nde1 promote the processive motility of mammalian dynein-dynactin in the presence of Lis1. This promotive effect is through tethering of Lis1 to dynein, as Nde1 mutants that cannot bind Lis1 or dynein failed to stimulate dynein motility. In comparison, excess Nde1 inhibited the assembly of the DDR complex and Nde1 was released from dynein before the initiation of DDR motility. In addition to the tethering mechanism, Nde1 binding rescues Lis1 from its antagonistic regulator, the α2 subunit of platelet-activating factor acetylhydrolase (PAF-AH)[51]. Our results illuminate the physiological function of this key regulatory protein in the dynein pathway.

Results

Nde1 is a biphasic regulator of dynein together with Lis1

To investigate how Nde1 regulates dynein, we reconstituted the assembly of wild-type (WT) human dynein in the presence of pig brain dynactin, and LD655-labeled mouse BicDR1 adaptor on surface-immobilized microtubules in vitro and monitored the motility of processive DDR

complexes using a total internal reflection fluorescence (TIRF) imaging assay (Fig. 1a). In the absence of Lis1, we observed processive runs of the DDR complexes assembled with WT dynein (wtDDR) at low frequency, consistent with autoinhibition of dynein. The addition of 20 nM unlabeled Nde1 in the absence of Lis1 did not substantially affect the frequency of processive runs, but the addition of excess (2,000 nM) Nde1 almost fully inhibited wtDDR motility (Fig. 1b, c), consistent with Nde1 overexpression to disrupt dynein-dependent functions in cells[21, 36, 42, 43].

We next tested how Nde1 addition affects dynein motility in the presence of Lis1. Consistent with previous reports that Lis1 facilitates the assembly of the DDR complexes and increases the likelihood of dynactin to recruit two dyneins[16, 17], Lis1 addition increased the run frequency of wtDDR by up to 2.6 fold and resulted in faster motility in the absence of Nde1 (Fig. 1d, e and Supplementary Fig. 1). Remarkably, the addition of 2 - 20 nM Nde1 resulted in up to 16-fold increase in run frequency in the presence of Lis1 (Fig. 1d, e, Supplementary Fig. 1a, and Supplementary Movie 1), demonstrating that Lis1 and Nde1 synergistically promote the activation of dynein motility. Nde1 addition also led to a modest increase in the average velocity of processive runs (Supplementary Fig. 1b), indicating that Nde1 further enhances the recruitment of two dyneins to dynactin.

We tested whether higher concentrations of Nde1 further enhance dynein motility. Unlike this expectation, 500 nM Nde1 substantially lowered the run frequency, and 2,000 nM Nde1 almost fully inhibited dynein motility in the presence of 20–500 nM Lis1 (Fig. 1d, e, and Supplementary Fig. 1a). These results indicate that Nde1 is a biphasic regulator of dynein: low concentration (2 - 20 nM) of Nde1 is sufficient to enhance dynein motility together with Lis1, whereas excess Nde1 inhibits dynein independent of Lis1.

To distinguish between these two opposing effects of Nde1, we repeated our measurements using a dynein mutant unable to attain the phi conformation[6]. Consistent with our previous measurements [16], the addition of 100 nM Lis1 only slightly (1.2 fold) increased the run frequency of DDR complexes assembled with mutant dynein (mtDDR, Fig. 1f, Supplementary Fig. 2, and Supplementary Movie 2). Unlike wtDDR, the run frequency of mtDDR exhibited little to no increase (1.1-fold) upon the addition of 20 nM Nde1 together with 100 nM Lis1. However, similar to wtDDR, the addition of excess Nde1 almost fully abolished mtDDR motility in the presence of Lis1 (Fig. 1f, g). These results indicate that a low concentration of Nde1 is sufficient for a more effective release of dynein from its autoinhibited conformation by Lis1, whereas inhibition of dynein by excess Nde1 is not related to the autoinhibitory mechanism of dynein. We also noticed the run frequency of wtDDR becomes nearly equivalent to that of mtDDR only in the presence of Lis1 and low concentration (20 nM) of Nde1 (Fig. 1g), indicating that both Lis1 and Nde1 are required for efficiently rescuing dynein from its autoinhibited conformation.

The activation of dynein by Nde1 is by the recruitment of dimerized Lis1 to dynein

We next turned our attention to determine how Nde1 facilitates Lis1-mediated activation of dynein motility. The N-terminal coiled-coil of Nde1 has high sequence conservation among different species and contains distinct binding sites for Lis1 and DIC [52]. The C-terminus of Nde1

is predicted to contain a short coiled-coil domain flanked with intrinsically disordered regions and has been reported to bind to the dynein heavy chain [35, 53]. Using AlphaFold2[54, 55], we modeled Lis1 binding to Nde1. The model predicted that Lis1 binds to the N-terminal coiled-coil domains of Nde1 with both of its β-propeller domains, and the C-terminal coiled-coil of Nde1 folds back to the N-terminal coiled-coil domain at a position near the Lis1 binding site (Fig. 2a and Supplementary Movie 3), raising the possibility of interference of this region with Lis1 binding. To distinguish whether the N-terminal coiled-coil of Nde1 is sufficient or the C-terminus also contributes to the regulatory role of Nde1 in the dynein activation pathway, we first used mass photometry to determine the oligomeric state and Lis1 association of full-length and C-terminal truncated ($Nde1^{1-190}$) Nde1 constructs (Fig. 2b and Supplementary Fig. 3). Both Nde1 and $Nde1^{1-190}$ form a homodimer [29, 56] and interact with a Lis1 dimer at 1:1 or 1:2 ratios (Fig. 2b). $Nde1^{1-190}$ interacted with Lis1 more efficiently than Nde1 (59% versus 29% of the total population), indicating that the Nde1 C-terminus may negatively regulate Lis1 binding to Nde1 (Fig. 2b). Similar to Nde1, motility assays showed that $Nde1^{1-190}$ biphasically regulated wtDDR motility in the presence of Lis1 (Fig. 2c, d), indicating that the N-terminal coiled-coil is sufficient for both the activating and inhibitory effects of Nde1 on dynein motility.

The previous studies proposed that the primary role of Nde1 is to tether Lis1 to dynein [12, 26, 30, 36, 37, 57]. To test this model, we immobilized Alexa488-labeled WT dynein from its tail to a coverslip and determined the colocalization of LD555-labeled Lis1 to dynein in the presence and absence of Nde1. Consistent with this model, we observed that increasing the Nde1 concentration from 0 to 10 nM substantially increased the colocalization of Lis1 to surface-immobilized dynein (Fig. 2e, f and Supplementary Fig. 4a). Similarly, co-immunoprecipitation (Co-IP) assays showed higher Lis1 binding to dynein under increasing concentrations of Nde1 (Supplementary Fig. 4b).

Although the tethering mechanism proposes that Lis1, Nde1, and dynein form a ternary complex, our Alphafold2 model predicts that Lis1 interacts with Nde1 through the same surface of its β-propeller domain that interacts with dynein[15, 58], raising doubts on whether Lis1 can simultaneously interact with dynein and Nde1. To test this possibility, we expressed a well-established dynein-binding mutant (R316A and W340A mutations on the β-propeller domain) of Lis1 (mtLis1, Fig. 3a)[17]. These mutations did not affect Lis1 dimerization but substantially reduced Lis1 binding to dynein and Nde1 in both single-molecule colocalization and Co-IP assays (Fig. 3b-d, Supplementary Fig. 5a). We also did not observe a combined peak of mtLis1 and $Nde1^{1-190}$ in mass photometry (Fig. 3e), demonstrating that dynein and Nde1 have overlapping binding sites on Lis1. mtLis1 also failed to enhance wtDDR motility in the presence or absence of Nde1 (Supplementary Fig. 5b, c), underscoring that binding of the β-propeller domain of Lis1 to dynein is essential for Lis1-mediated activation of dynein.

Despite overlapping binding sites of dynein and Nde1 on Lis1, we reasoned that a Lis1 dimer can still form a ternary complex with Nde1 and dynein with one β-propeller domain interacting with Nde1 and the other interacting with dynein. Consistent with this possibility, structural studies have shown that Lis1 binds to dynein primarily by one of its β-propeller domains near the AAA3 site, whereas the other β-propeller domain is either unbound or bound to dynein's stalk[15,

[59]. According to this scheme, Lis1 dimerization is essential for being tethered to dynein by Nde1. We tested this possibility by truncating the LisH domain of Lis1 at two positions ($Lis1^{39-410}$ and $Lis1^{83-410}$, Fig. 3a, Supplementary Fig. 5d). Mass photometry revealed that Lis1 forms a stable dimer, whereas $Lis1^{39-410}$ is only weakly (5%) dimerized and $Lis1^{83-410}$ is a monomer (Fig. 3b).

In single molecule colocalization assays, we observed that WT Lis1 can colocalize with dynein in the absence of Nde1, albeit at low efficiency (Fig. 2f), and it stimulates $Nde1^{1-190}$ association with dynein (Fig. 3f). This could be because purified dynein can be in either open or phi conformation[6], and Lis1 can interact with open dynein without Nde1. Unlike WT Lis1, $Lis1^{83-410}$ did not facilitate $Nde1^{1-190}$ association with dynein in single-molecule colocalization assays (Fig. 3f). In the absence of Nde1, 100 nM of $Lis1^{39-410}$ or $Lis1^{83-410}$ increased the run frequency of wtDDR by ~2-fold, comparable to 100 nM Lis1 (Fig. 3g, h), underscoring that a Lis1 monomer is sufficient to enhance activation of dynein motility[17]. While the addition of 20 nM Nde1 boosts the wtDDR run frequency with Lis1 by more than 10-fold, Nde1 addition resulted in a modest (3.2-fold) increase in run frequency with $Lis1^{39-410}$ and had no significant effect on dynein run frequency when added together with $Lis1^{83-410}$ (Fig. 3g, h). Collectively, these results are consistent with the ability of Lis1 dimer to simultaneously interact with Nde1 and dynein and indicate that Lis1 dimerization is essential for Nde1 to enhance the Lis1-mediated activation of dynein.

Excess Nde1 inhibits DDR formation by competing with dynactin for DIC

We next investigated the inhibitory effect of Nde1 on dynein motility. Previous studies have shown that the N-terminal coiled-coil of Nde1 binds to DIC, and that Nde1 binding overlaps with the binding of the p150 subunit of dynactin to DIC [31, 37, 38, 45, 46]. While the physiological role of the p150-DIC interaction remains elusive, it is possible that excess Nde1 competes against p150 binding to DIC and disrupts the assembly of active DDR complexes. Alternatively, Nde1 may directly inhibit subsequent motility after the complexes have been assembled through its reported interaction with the dynein motor domain. To distinguish between these possibilities, we added excess Nde1 before or after we mixed WT dynein, dynactin, and BiDR1 and tested wtDDR motility. The addition of Nde1 before DDR assembly resulted in a significant decrease in run frequency, while Nde1 addition after the assembly did not have a significant effect on wtDDR run frequency (Fig. 4a, b). Therefore, excess Nde1 impedes dynein motility by preventing DDR formation, rather than inhibiting the motility of pre-assembled complexes on microtubules.

To understand why excess Nde1 does not inhibit the complexes that are walking along microtubules, we monitored the association of fluorescently labeled Nde1 with dynein in single-molecule assays. If Nde1 can still associate with DIC, but its binding does not affect the motility of dynein already assembled with dynactin, we expected to observe colocalization of Nde1 to processive wtDDR complexes. While 70% of DDR complexes co-migrated with Lis1, only less than 10% comigrated with Nde1 in three-color TIRF assays (Fig. 4c, d). This observation indicates that Nde1 and p150 binding to DIC are mutually exclusive and Nde1 cannot bind to dynein assembled with dynactin.

If Nde1 and dynactin binding to DIC are mutually exclusive, we anticipated dynactin binding to release Nde1 from dynein before the initiation of DDR motility. To test this possibility, we first determined colocalization of LD655-Nde1 to GFP-dynein on surface-immobilized microtubules, and while imaging, introduced dynactin and BicDR1 to initiate DDR motility in the absence of Lis1 (Fig. 4e). Out of the Nde1 spots that colocalized with dynein, 96% were released before the initiation of DDR motility (Fig. 4f-i) and more than half of dyneins started to move processively toward the minus-end within 2 s after the release of Nde1 (Fig. 4g), indicating that dynactin binding causes Nde1 to release from dynein. When we performed the flow assay in the presence of Lis1, we observed only 50% of Nde1 to release from dynein while the other half comigrated with DDR on microtubules (Fig. 4h, i). Therefore, Nde1 can remain indirectly associated with motile DDR complexes via Lis1 during the initiation of dynein motility. This indirect association is likely to be transient as we observe only 10% of DDR complexes to comigrate with Nde1 when Lis1 and Nde1 were preincubated with DDR components (Fig. 4c, d).

To conclusively reveal how dynein binding and Lis1 binding of Nde1 contribute to the biphasic regulation of dynein motility, we generated Nde1 mutants that either cannot bind to DIC or Lis1. The point mutation to E47 of Nde1 has been shown to inhibit its binding to DIC[36]. Based on previous mutagenesis studies of Ndel1[29, 36] and our AlphaFold2 model, we mutated the residues that facilitate Nde1 binding to Lis1 (E118 and R129) (Fig. 2a). We generated both alanine ($Nde1^{E47A}$ and $Nde1^{E118A/R129A}$) and charge reversal ($Nde1^{E47K}$ and $Nde1^{E118K/R129E}$) substitutions to selectively disrupt Lis1 and DIC binding of Nde1 (Fig. 5a). Motility assays showed that, unlike Nde1, none of the Nde1 mutants (20 nM) enhanced the run frequency of wtDDR in the presence of Lis1 (Fig. 5b, c and Supplementary Movie 4), showing that both Lis1 and DIC binding of Nde1 are required for Lis1-mediated activation of dynein. We then tested the inhibitive effect of 500 nM Nde1 mutants in the absence of Lis1. Both WT and Lis1-binding mutants of Nde1 decreased the frequency of mtDDR runs by ~50% compared to the no Nde1 condition (Fig. 5d, e). However, DIC-binding mutants of Nde1 did not affect the run frequency (Fig. 5d, e), further supporting our conclusion that excess Nde1 competes with dynactin for DIC binding and negatively regulates the formation of the DDR complex.

Nde1 and PAF-AH α2 antagonistically regulate Lis1

Lis1 has been initially identified as the noncatalytic β subunit of PAF-AH [60] and the catalytically-active α1 and α2 subunits of PAF-AH have been suggested? to inactivate dynein by interacting with Lis1[51]. Nde1 overexpression rescued this inhibition by competing against α2 for Lis1-binding [51]. Nde1 has been shown to compete with α2 to bind Lis1 [14], but it remained unclear how Nde1 and α2 regulate the Lis1-mediated activation of dynein. To address these questions, we assayed the competitive binding of α2 and Nde1 using purified components and determined how α2 affects the regulation of DDR motility by Lis1/Nde1. Previously reported structures of DHC-Lis1[61] and α2-Lis1 [14], together with our AlphaFold2 model of Nde1-Lis1 show that dynein, α2, and Nde1 share the same binding site on Lis1 (Fig. 6a). Consistent with this model, mass photometry assays showed that α2 forms a complex with Lis1 but does not bind mtLis1 that interacts with neither dynein nor $Nde1^{1-190}$ (Fig. 6b). In addition, Lis1 cannot form a ternary complex with α2 and $Nde1^{1-190}$ (Fig. 6b). Single-molecule colocalization assays also

showed that Lis1 exhibits reduced colocalization to both dynein and Nde1 under the increasing concentration of α2 (Fig. 6c).

Single-molecule motility assays showed that, in the absence of Nde1 and Lis1, α2 does not directly alter the run frequencies of wtDDR or mtDDR (Supplementary Fig. 6). However, α2 addition lowers the wtDDR run frequency in a dose-dependent manner in the presence of Lis1 (Fig. 6d-f), demonstrating that α2 downregulates Lis1 function by preventing its interaction with dynein. We also observed dose-dependent inhibition of wtDDR by α2 and activation by Nde1 over a wide range of concentrations (0 - 100 nM), indicating that Nde1 rescues Lis1 from inhibition by α2 and tethers it to dynein (Fig. 6g, h). Consistent with this conclusion, premixing Lis1 and α2 before DDR assembly decreases the run frequency compared to the Lis1-only condition, but this can be rescued by Nde1 addition during complex assembly (Supplementary Fig. 7). These results show that Nde1 facilitates dynein motility by rescuing Lis1 from α2 inhibition.

Discussion

In this study, we investigated how Nde1 functions together with Lis1 to regulate dynein by reconstituting the motility of DDA complexes. We showed that Nde1 rescues Lis1 from its antagonist, the α2 subunit of PAF-AH, and substantially increases Lis1 binding to dynein in the absence of dynactin and an adaptor protein. While Lis1 alone increases the frequency of wtDDR runs by ~3-fold, Nde1 and Lis1 together increase the run frequency up to 16-fold. This dramatic increase in the run frequency of WT dynein was similar to that of a phi mutant of dynein that effectively forms a complex with dynactin and BicDR1 in the absence of regulatory factors[6]. Therefore, we concluded that both Nde1 and Lis1 are needed to efficiently activate autoinhibited dynein. Besides its activating role, we observed Nde1 alone or excess Nde1 in the presence of Lis1 to inhibit dynein motility. By selectively disrupting Lis1 and DIC binding of Nde1, we showed that the inhibitory role of Nde1 is related to its binding to DIC and is independent of its binding to Lis1.

Based on our results, we propose a mechanistic model of how Nde1 functions in the dynein activation pathway together with Lis1 (Fig. 7). Key features of this model are the binding of Nde1, α2, and dynein to the same site on the β-propeller domain of Lis1 [14, 15] and overlapping binding of the N-terminal coiled-coil of Nde1 and the p150 subunit of dynactin to DIC [31, 37, 38, 45, 46]. The assembly of processive DDA complexes requires the opening of phi dynein[6]. Rescue of dynein from autoinhibited conformation is primarily driven by Lis1 binding to the AAA+ ring of dynein[11, 16-18, 40]. However, Lis1 does not strongly interact with autoinhibited dynein because the Lis1 binding site at the AAA3 site appears inaccessible in the phi conformation[11, 17, 18]. In addition, Lis1 binding to dynein can be inhibited by α2 binding to Lis1[51]. Nde1 facilitates the interaction of Lis1 with dynein in two distinct steps. First, Nde1 effectively competes against α2 binding to Lis1, rescuing Lis1 from inhibition. Second, Nde1 tethers Lis1 to dynein by simultaneously interacting with Lis1 and DIC. While the Nde1 binding site of DIC has not been observed in available structures of the dynein complex[62], we hypothesize that Nde1 can access DIC and efficiently tether Lis1 to phi dynein. Although dynein and Nde1 bind to the same site on the β-propeller domain of Lis1, we reason that Lis1 can simultaneously interact with Nde1 and

dynein with its two β propeller domains. Consistent with this view, we showed that two Lis1 dimers can simultaneously bind to an Nde1 dimer (Fig. 2b, 10%-12% of the total population), In addition, a single Lis1 β propeller promotes dynein activation[17] comparable to our Lis1-only condition, but we did not observe Nde1-mediated enhancement of dynein activation when added together with a single Lis1 β propeller. Collectively, we propose that the formation of the dynein-Lis1-Nde1 ternary complex is a key intermediate in the dynein activation pathway.

Tethering Lis1 increases its local concentration and may enable more efficient binding of Lis1 to the AAA3 site upon transient opening of phi dynein or directly triggers the opening of phi dynein by wedging between the two AAA+ rings of a dynein dimer[63]. Open dynein interacts with dynactin and a cargo adaptor to form an active complex. However, the interaction between the p150 subunit and the N-terminus of DIC is critical for dynactin binding to dynein [64]. Because p150 and Nde1 have overlapping binding sites on DIC, Nde1 binding to DIC is incompatible with DDA assembly and Nde1 is released from DIC before the initiation of processive motility (Fig. 7). While Lis1 remains bound to most of processive DDA complexes in our assay conditions, it is not required for DDA motility, and either Nde1 dissociation from DIC or activation of dynein processivity[65] may also trigger the subsequent release of Lis1 from dynein.

Our model provides a mechanistic explanation for seemingly conflicting observations made for Nde1 and Lis1 in vivo and in vitro. While cell based-assays showed that Nde1 is crucial for the recruitment of Lis1 to activate dynein [26, 35, 38, 53, 66], several in vitro studies showed Nde1 inhibits dynein [30, 47]. We showed that Nde1 serves as both the positive and negative regulator of dynein, resulting in biphasic regulation of the dynein activation pathway. Biphasic regulation arises because activating and inhibitory effects dominate at different Nde1 concentrations. We showed that a relatively low concentration of Nde1 is sufficient to tether Lis1 to dynein, increasing its apparent affinity for dynein. This could be a critical step for endogenous Lis1 to bind dynein, as haploinsufficiency of Lis1 causes lissencephaly[38]. Our results are also consistent with observations that Ndel1 depletion can be rescued by overexpression of Lis1, but Ndel1 overexpression cannot rescue Lis1 deletion [36]. Excess Lis1 may efficiently interact with dynein and stimulate DDA assembly even in the absence of Nde1. In comparison, without Lis1, Nde1 is incapable of activating dynein and instead plays an inhibitory role by competing against DIC-dynactin interaction. We also observed excess Nde1 to inhibit dynein activation even in the presence of Lis1, providing a possible explanation for why excess Nde1 has a deleterious effect on dynein function in cells [21, 36, 42, 43].

Our results are also largely consistent with two concurrent in vitro studies, which reported that Ndel1 tethers Lis1 to dynein and competes against p150 binding to dynactin[64, 67]. While Garrott et al. [67] also reported Nde1 disfavors the formation of active DDA complexes, they did not observe activating role of Ndel1 in dynein motility when added together with Lis1. This discrepancy could be related to the differences in Nde1 paralogs (Nde1 vs. Ndel1) and activating adaptors (BiCDR1 vs. BicD2), and possible differences in affinities of purified proteins used in our studies. Future studies are required to distinguish between similar but potentially distinct cellular roles of Nde1 and Ndel1, as deletion of Nde1 causes microcephaly while the loss of Ndel1 is usually fatal[28]. We also note that Nde1/Ndel1 have been reported to interact with other

cellular factors [28] and it remains to be demonstrated whether these proteins recruit additional regulatory factors to the dynein transport machinery.

Methods

Protein expression and purification

The plasmids with the pOmniBac backbone were transformed into DH10Bac competent cells and plated onto Bacmid plates with BluoGal at 37 °C for 2 days. A white colony was selected and grown in 2X-YT media overnight. Bacmid plasmids were purified and transfected onto adherent SF9 cells. The transfected SF9 cells were incubated at 27 °C for 3 days to grow the p1 virus. Then 2 mL of p1 virus was added to 50 mL suspended SF9 cell culture and incubated at 27 °C in a shaking incubator for 3 days to obtain the p2 virus. Then p2 virus was collected by centrifuging at 4,000 *g* for 10 min and stored at 4 °C in dark for long-term use.

For protein expression, 1 L suspended SF9 cell culture was infected by the p2 virus with the multiplicity of infection (MOI) at 3 and incubated for 3 days. Cells were collected by centrifuging at 4,000 *g* for 10 min. Then the pellets were either immediately lysed for protein purification or snap-frozen in liquid nitrogen and stored at -80°C.

To extract proteins, SF9 pellets were re-suspended into the lysis buffer (25 mM HEPES pH 7.4, 150 mM KAc, 1 mM $MgCl_2$, 1 mM EGTA, 1 mM DTT, 0.1 mM ATP, 20 mM PMSF, and 10 Roche protease inhibitor tablets per L) and lysed by a dounce homogenizer. Lysate was cleared at 150,000 *g* for 30 min in a Ti70 rotor (Beckman Coulter) and the supernatant was incubated with 1 mL IgG Sepharose beads (GE Healthcare) for 1 h at 4 °C. The beads were collected and washed with lysis buffer and then with the TEV buffer (25 mM HEPES pH 7.4, 150 mM KAc, 1 mM $MgCl_2$, 1 mM EGTA, 1 mM DTT, 0.1 mM ATP). To elute the proteins from the beads, 0.1 mg/mL TEV protease was added and rolled at a nutator for 1 h at room temperature. Proteins were separated from the beads using a 0.45 µm pore-sized centrifugation filter (Amicon Ultrafree MC) and concentrated with 50K MWCO concentrators (Amicon).

For fluorescent labeling, proteins were incubated with 4-fold excess dye derivatized with either benzylguanine (BG, for SNAP labeling) or coenzyme A (CoA, for ybbR labeling) at 37°C for 1 h. Dynein was labeled at room temperature. 5 µM SFP enzyme was added to catalyze ybbR labeling with CoA. Labeled proteins in TEV buffer were eluted from a size exclusion column to remove the free dye and other impurities. Dynein was eluted from TSKgel G4000SWXL column (Tosoh), BicDR1 was eluted from Superose 6 10/300 GL column (Cytiva), whereas Lis1, Nde1, and α2 were eluted from the Superdex 200 Increase 10/300 GL column (Cytiva) (Supplementary Fig. 8).

Dynactin was purified from pig brains using SP Sepharose Fast Flow and MonoQ ion exchange columns (Cytiva) and the TSKgel G4000SWXL size exclusion column (Tosoh), as previously described [68]. Dynactin was labeled with LD555 derivatized with NHS and excess dye was removed by passing the dynactin solution through a desalting column (Zeba).

Microscopy

The fluorescent imaging was performed with a custom-built multicolor objective-type TIRF microscope equipped with a Nikon Ti-E microscope body, a 100X magnification 1.49 N.A. apochromatic oil-immersion objective (Nikon) together with a Perfect Focus System. The

fluorescence signal was detected using an electron-multiplied charge-coupled device camera: (Andor, Ixon EM^+, 512 × 512 pixels). The effective camera pixel size after magnification was 160 nm. Alexa488/GFP/mNeonGreen, LD555, and LD655 probes were excited using 488 nm, 561 nm, and 633 nm laser beams (Coherent) coupled to a single model fiber (Oz Optics), and their emission was filtered using 525/40, 585/40, and 655/40 band path filters (Semrock), respectively. The microscope was controlled by MicroManager 1.4.

Preparation of Flow Chambers

We used PEG-biotin-coating of glass coverslips to reduce the nonspecific binding of proteins to the glass surface, as described[69]. Briefly, plain glass coverslips were cleaned with water, acetone, and water sequentially, and then sonicated in a 1 M KOH using a bath sonicator. The coverslips were then rinsed with water, incubated in 3-Aminopropyltriethoxysilane in acetate and methanol for 10 min before and after a 1-min sonication, cleaned with methanol, and air-dried. 30 µl of biotin-PEG-SVA (biotin-polyethylene glycol valeric acid) in a $NaHCO_3$ buffer (pH 7.4) was sandwiched by two pieces of coverslips at 4 °C overnight. The coverslips were cleaned with water and air-dried, vacuum sealed, and kept at -20 °C for long-term storage. Flow chambers were built by sandwiching a double-sided tape with a PEG-coated coverslip and a glass slide. To flow a solution into a flow chamber while recording DDR motility in real time, two holes were drilled at each end of the chamber on the glass slides.

Single-molecule motility assays

The flow chambers were incubated with 5 mg ml^{-1} streptavidin for 2 min and washed with MB buffer (30 mM HEPES pH 7.0, 5 mM $MgSO_4$, 1 mM EGTA, 1 mg ml^{-1} casein, 0.5% pluronic acid, 0.5 mM DTT, and 1 µM Taxol). The chamber was then incubated with biotinylated microtubules for 2 min and washed with MB buffer. Proteins were diluted and mixed into desired concentrations in MB buffer. For DDR assembly, 10 nM dynein, 150 nM dynactin, and 100nM BicDR1 were incubated on ice for 25 min and then diluted 10-fold into imaging buffer (MB buffer supplemented with 0.1 mg ml^{-1} glucose oxidase, 0.02 mg ml^{-1} catalase, 0.8% D-glucose, and 2 mM ATP), introduced to the flow chamber, motility was recorded for 5 min.

Single-molecule colocalization assays were performed by labeling the SNAP-tagged "bait" protein (either dynein or Lis1) with equal concentrations of Alexa488-BG and biotin-BG. Biotin-PEG coated flow chamber was incubated with 5 mg ml^{-1} streptavidin for 2 min and washed with MB buffer. Then the bait protein was diluted into 2 nM in MB buffer and incubated in the chamber for 1 min. Then the chamber was washed with MB buffer. The "prey" proteins were labeled with LD655, diluted in MB buffer, flowed into the chamber, and incubated for 10 min. The fluorescence signals of Alexa488 and LD655 were recorded without washing away the unbound prey proteins in the solution.

Co-Immunoprecipitation

GFP tageed proteins were labeled with Alexa-488 for Typhoon imaging in Comassie gel. GFP-Trap beads (Chromotek) were incubated with MB buffer supplemented with 5 mg ml^{-1} BSA overnight at 4 °C to minimize non-specific binding. Proteins were mixed with Co-IP buffer (MB

buffer supplemented with 5mg ml^{-1} BSA and 150 mM NaCl) and diluted into desired concentrations. 20% of the protein mix was separated into another tube as "Input". The remaining 80% was incubated with GFP-Trap beads and incubated for 1 h on ice. The beads were then washed with Co-IP buffer and centrifuged at 2,000 *g* for 3 min three times to remove unbound protein in the supernatant. Input and beads were run in a denaturing gel (NuPAGE, Thermofisher). The gel was imaged using GF Typhoon FLA 9500A to detect the fluorescence signal of the labeled proteins that eluted with the beads.

Mass photometry

High-precision coverslips (Azer Scientific) were cleaned with isopropanol and water alternatively 3 times in a bath sonicator and air-dried. The gasket was cleaned with isopropanol and water alternatively 3 times without sonication, air-dried, and placed onto a clean coverslip. 14 µL of mass photometry buffer (30 mM HEPES pH 7.4, 5 mM $MgSO_4$, and 1 mM EGTA, 10% glycerol) was loaded onto a well for the autofocus. The protein sample was diluted into 8 nM in mass photometry buffer and added to the coverslips. Protein contrast count was collected with a TwoMP mass photometer of Refeyn 2 with two technical replicates. Mass measurements of the instrument were calibrated using the standard mix (conalbumin, aldolase, and thyroglobulin).

Data analysis

The run frequency was calculated by observing the number of processive BicDR1 on each microtubule divided by the length of the microtubule and the duration of data collection using a custom-written MATLAB code. Velocity was calculated by detecting the start and the end of each processive run of BicDR1. The fraction of single molecule colocalization was calculated by dividing the number of LD655 spots that colocalize with Alexa488 by the total number of Alexa 488 spots on the 40 µm x 40 µm imaging area. Colocalization was defined as the maximum 300 nm distance between the peaks of diffraction-limited spots of Alexa488 and LD6555 dyes. The localization of dyes was detected by a modified version of FIESTA [70] (YFIESTA, available on https://github.com/Yildiz-Lab/YFIESTA).

AlphaFold2 protein structure prediction

AlphaFold2 structure prediction for $Nde1^{1-190}$-Lis1 and Nde1 was performed on Google ColabFold with AlphaFold2_mmseqs2 version (available on https://github.com/sokrypton/ColabFold) using default settings. The structure of Nde1-Lis1 was generated with structural alignment of $Nde1^{1-190}$-Lis1 and Nde1 structure prediction based on the 1-180 AA of Nde1. The images and movies of the structural models were created on the RCSB website.

References

1. Reck-Peterson, S.L., Redwine, W.B., Vale, R.D. & Carter, A.P. The cytoplasmic dynein transport machinery and its many cargoes. *Nat Rev Mol Cell Bio* **19**, 382-398 (2018).
2. King, S.M. *Dynein Mechanics, Dysfunction, and Disease*. (Academic Press, London, England; 2018).
3. Canty, J.T., Tan, R., Kusakci, E., Fernandes, J. & Yildiz, A. Structure and mechanics of dynein motors. *Annual review of biophysics* **50**, 549-574 (2021).
4. Tan, Z. *et al.* Autoinhibited kinesin-1 adopts a hierarchical folding pattern. *BioRxiv*, 2023.2001.2026.525761 (2023).
5. Trokter, M., Mucke, N. & Surrey, T. Reconstitution of the human cytoplasmic dynein complex. *P Natl Acad Sci USA* **109**, 20895-20900 (2012).
6. Zhang, K. *et al.* Cryo-EM Reveals How Human Cytoplasmic Dynein Is Auto-inhibited and Activated. *Cell* **169**, 1303-1314 (2017).
7. Splinter, D. *et al.* BICD2, dynactin, and LIS1 cooperate in regulating dynein recruitment to cellular structures. *Mol Biol Cell* **23**, 4226-4241 (2012).
8. McKenney, R.J., Huynh, W., Tanenbaum, M.E., Bhabha, G. & Vale, R.D. Activation of cytoplasmic dynein motility by dynactin-cargo adapter complexes. *Science* **345**, 337-341 (2014).
9. Schlager, M.A., Hoang, H.T., Urnavicius, L., Bullock, S.L. & Carter, A.P. In vitro reconstitution of a highly processive recombinant human dynein complex. *Embo J* **33**, 1855-1868 (2014).
10. Urnavicius, L. *et al.* The structure of the dynactin complex and its interaction with dynein. *Science* **347**, 1441-1446 (2015).
11. Markus, S.M., Marzo, M.G. & McKenney, R.J. New insights into the mechanism of dynein motor regulation by lissencephaly-1. *Elife* **9**, e59737 (2020).
12. Huang, J., Roberts, A.J., Leschziner, A.E. & Reck-Peterson, S.L. Lis1 Acts as a "Clutch" between the ATPase and Microtubule-Binding Domains of the Dynein Motor. *Cell* **150**, 975-986 (2012).
13. Kim, M.H. *et al.* The structure of the N-terminal domain of the product of the lissencephaly gene Lis1 and its functional implications. *Structure* **12**, 987-998 (2004).
14. Tarricone, C. *et al.* Coupling PAF signaling to dynein regulation: Structure of LIS1 in complex with PAF-Acetylhydrolase. *Neuron* **44**, 809-821 (2004).
15. Gillies, J.P. *et al.* Structural basis for cytoplasmic dynein-1 regulation by Lis1. *Elife* **11**, e71229 (2022).
16. Elshenawy, M.M. *et al.* Lis1 activates dynein motility by modulating its pairing with dynactin. *Nat Cell Biol* **22**, 570-578 (2020).
17. Htet, Z.M. *et al.* LIS1 promotes the formation of activated cytoplasmic dynein-1 complexes. *Nat Cell Biol* **22**, 518-525 (2020).
18. Marzo, M.G., Griswold, J.M. & Markus, S.M. Pac1/LIS1 stabilizes an uninhibited conformation of dynein to coordinate its localization and activity. *Nat Cell Biol* **22**, 559-569 (2020).
19. Jha, R., Roostalu, J., Cade, N.I., Trokter, M. & Surrey, T. Combinatorial regulation of the balance between dynein microtubule end accumulation and initiation of directed motility. *Embo J* **36**, 3387-3404 (2017).
20. Lenz, J.H., Schuchardt, I., Straube, A. & Steinberg, G. A dynein loading zone for retrograde endosome motility at microtubule plus-ends. *Embo J* **25**, 2275-2286 (2006).
21. Stehman, S.A., Chen, Y., McKenney, R.J. & Vallee, R.B. NudE and NudEL are required for mitotic progression and are involved in dynein recruitment to kinetochores. *J Cell Biol* **178**, 583-594 (2007).

22. Pandey, J.P. & Smith, D.S. A Cdk5-Dependent Switch Regulates Lis1/Ndel1/Dynein-Driven Organelle Transport in Adult Axons. *J Neurosci* **31**, 17207-17219 (2011).
23. Yi, J.Y. *et al.* High-resolution imaging reveals indirect coordination of opposite motors and a role for LIS1 in high-load axonal transport. *J Cell Biol* **195**, 193-201 (2011).
24. Egan, M.J., Tan, K.L. & Reck-Peterson, S.L. Lis1 is an initiation factor for dynein-driven organelle transport. *J Cell Biol* **197**, 971-982 (2012).
25. Dix, C.I. *et al.* Lissencephaly-1 promotes the recruitment of dynein and dynactin to transported mRNAs. *J Cell Biol* **202**, 479-494 (2013).
26. Wang, S.S. *et al.* Nudel/NudE and Lis1 promote dynein and dynactin interaction in the context of spindle morphogenesis. *Mol Biol Cell* **24**, 3522-3533 (2013).
27. Moughamian, A.J., Osborn, G.E., Lazarus, J.E., Maday, S. & Holzbaur, E.L.F. Ordered Recruitment of Dynactin to the Microtubule Plus-End is Required for Efficient Initiation of Retrograde Axonal Transport. *J Neurosci* **33**, 13190-13203 (2013).
28. Garrott, S.R., Gillies, J.P. & DeSantis, M.E. Nde1 and Ndel1: Outstanding Mysteries in Dynein-Mediated Transport. *Front Cell Dev Biol* **10**, 871935 (2022).
29. Derewenda, U. *et al.* The structure of the coiled-coil domain of Ndel1 and the basis of its interaction with Lis1, the causal protein of Miller-Dieker lissencephaly. *Structure* **15**, 1467-1481 (2007).
30. McKenney, R.J., Vershinin, M., Kunwar, A., Vallee, R.B. & Gross, S.P. LIS1 and NudE Induce a Persistent Dynein Force-Producing State. *Cell* **141**, 304-314 (2010).
31. Nyarko, A., Song, Y.J. & Barbar, E. Intrinsic Disorder in Dynein Intermediate Chain Modulates Its Interactions with NudE and Dynactin. *J Biol Chem* **287**, 24884-24893 (2012).
32. Ye, F. *et al.* DISC1 Regulates Neurogenesis via Modulating Kinetochore Attachment of Ndel1/ Nde1 during Mitosis (vol 96, pg 1041, 2017). *Neuron* **96**, 1204-1204 (2017).
33. Tsai, J.W., Bremner, K.H. & Vallee, R.B. Dual subcellular roles for LIS1 and dynein in radial neuronal migration in live brain tissue. *Nat Neurosci* **10**, 970-979 (2007).
34. Lam, C., Vergnolle, M.A.S., Thorpe, L., Woodman, P.G. & Allan, V.J. Functional interplay between LIS1, NDE1 and NDEL1 in dynein-dependent organelle positioning. *J Cell Sci* **123**, 202-212 (2010).
35. Liang, Y. *et al.* Nudel functions in membrane traffic mainly through association with Lis1 and cytoplasmic dynein. *J Cell Biol* **164**, 557-566 (2004).
36. Wang, S.S. & Zheng, Y.X. Identification of a Novel Dynein Binding Domain in Nudel Essential for Spindle Pole Organization in Xenopus Egg Extract. *J Biol Chem* **286**, 587-593 (2011).
37. Zylkiewicz, E. *et al.* The N-terminal coiled-coil of Ndell is a regulated scaffold that recruits LIS1 to dynein. *J Cell Biol* **192**, 433-445 (2011).
38. Moon, H.M. *et al.* LIS1 controls mitosis and mitotic spindle organization via the LIS1-NDEL1-dynein complex. *Human molecular genetics* **23**, 449-466 (2014).
39. Wynne, C.L. & Vallee, R.B. Cdk1 phosphorylation of the dynein adapter Nde1 controls cargo binding from G2 to anaphase. *J Cell Biol* **217**, 3019-3029 (2018).
40. Qiu, R., Zhang, J. & Xiang, X. LIS1 regulates cargo-adapter-mediated activation of dynein by overcoming its autoinhibition in vivo. *J Cell Biol* **218**, 3630-3646 (2019).
41. Efimov, V.P. & Morris, N.R. The LIS1-related NUDF protein of Aspergillus nidulans interacts with the coiled-coil domain of the NUDE/RO11 protein. *J Cell Biol* **150**, 681-688 (2000).
42. Feng, Y.Y. *et al.* LIS1 regulates CNS lamination by interacting with mNudE, a central component of the centrosome. *Neuron* **28**, 665-679 (2000).
43. Ma, L. *et al.* Requirement for Nudel and dynein for assembly of the lamin B spindle matrix. *Nat Cell Biol* **11**, 247-256 (2009).

44. Monda, J.K. & Cheeseman, I.M. Nde1 promotes diverse dynein functions through differential interactions and exhibits an isoform-specific proteasome association. *Mol Biol Cell* **29**, 2336-2345 (2018).
45. McKenney, R.J., Weil, S.J., Scherer, J. & Vallee, R.B. Mutually Exclusive Cytoplasmic Dynein Regulation by NudE-Lis1 and Dynactin. *J Biol Chem* **286**, 39615-39622 (2011).
46. Jie, J., Lohr, F. & Barbar, E. Dynein Binding of Competitive Regulators Dynactin and NudE Involves Novel Interplay between Phosphorylation Site and Disordered Spliced Linkers. *Structure* **25**, 421-433 (2017).
47. Yamada, M. *et al.* LIS1 and NDEL1 coordinate the plus-end-directed transport of cytoplasmic dynein. *Embo J* **27**, 2471-2483 (2008).
48. Torisawa, T. *et al.* Functional Dissection of LIS1 and NDEL1 Towards Understanding the Molecular Mechanisms of Cytoplasmic Dynein Regulation. *J Biol Chem* **286**, 1959-1965 (2011).
49. Abdel-Hamid, M.S., El-Dessouky, S.H., Ateya, M.I., Gaafar, H.M. & Abdel-Salam, G.M.H. Phenotypic spectrum of NDE1-related disorders: from microlissencephaly to microhydranencephaly. *Am J Med Genet A* **179**, 494-497 (2019).
50. Torisawa, T. *et al.* Autoinhibition and cooperative activation mechanisms of cytoplasmic dynein. *Nat Cell Biol* **16**, 1118-1124 (2014).
51. Ding, C., Liang, X., Ma, L., Yuan, X. & Zhu, X. Opposing effects of Ndel1 and alpha1 or alpha2 on cytoplasmic dynein through competitive binding to Lis1. *J Cell Sci* **122**, 2820-2827 (2009).
52. Bradshaw, N.J., Hennah, W. & Soares, D.C. NDE1 and NDEL1: twin neurodevelopmental proteins with similar 'nature' but different 'nurture'. *Biomolecular concepts* **4**, 447-464 (2013).
53. Sasaki, S. *et al.* A LIS1/NUDEL/cytoplasmic dynein heavy chain complex in the developing and adult nervous system. *Neuron* **28**, 681-696 (2000).
54. Jumper, J. *et al.* Highly accurate protein structure prediction with AlphaFold. *Nature* **596**, 583-589 (2021).
55. Mirdita, M. *et al.* ColabFold: making protein folding accessible to all. *Nat Methods* **19**, 679-682 (2022).
56. Soares, D.C. *et al.* The Mitosis and Neurodevelopment Proteins NDE1 and NDEL1 Form Dimers, Tetramers, and Polymers with a Folded Back Structure in Solution. *J Biol Chem* **287**, 32381-32393 (2012).
57. Li, J., Lee, W.L. & Cooper, J.A. NudEL targets dynein to microtubule ends through LIS1. *Nat Cell Biol* **7**, 686-690 (2005).
58. Gutierrez, P.A., Ackermann, B.E., Vershinin, M. & McKenney, R.J. Differential effects of the dynein-regulatory factor Lissencephaly-1 on processive dynein-dynactin motility. *J Biol Chem* **292**, 12245-12255 (2017).
59. DeSantis, M.E. *et al.* Lis1 Has Two Opposing Modes of Regulating Cytoplasmic Dynein. *Cell* **170**, 1197-1208 (2017).
60. Hattori, M., Adachi, H., Tsujimoto, M., Arai, H. & Inoue, K. Miller-Dieker Lissencephaly Gene Encodes a Subunit of Brain Platelet-Activating-Factor. *Nature* **370**, 216-218 (1994).
61. Reimer, J.M., DeSantis, M.E., Reck-Peterson, S.L. & Leschziner, A.E. Structures of human dynein in complex with the lissencephaly 1 protein, LIS1. *Elife* **12**, e84302 (2023).
62. Chaaban, S. & Carter, A.P. Structure of dynein-dynactin on microtubules shows tandem adaptor binding. *Nature* **610**, 212-216 (2022).
63. Karasmanis, E.P. *et al.* Lis1 relieves cytoplasmic dynein-1 auto-inhibition by acting as a molecular wedge. *bioRxiv*, 2022.2010. 2010.511666 (2022).
64. Okada, K. *et al.* Conserved Roles for the Dynein Intermediate Chain and Ndel1 in Assembly and Activation of Dynein. *bioRxiv*, 2023.2001. 2013.523097 (2023).

65. Ton, W.D. *et al.* Microtubule binding-induced allostery promotes LIS1 dissociation from dynein prior to cargo transport. *bioRxiv*, 2022.2011. 2008.515461 (2022).
66. Shu, T. *et al.* Ndel1 operates in a common pathway with LIS1 and cytoplasmic dynein to regulate cortical neuronal positioning. *Neuron* **44**, 263-277 (2004).
67. Garrott, S.R. *et al.* Ndel1 modulates dynein activation in two distinct ways. *bioRxiv*, 2023.2001. 2025.525437 (2023).
68. King, S.J. & Schroer, T.A. Dynactin increases the processivity of the cytoplasmic dynein motor. *Nat Cell Biol* **2**, 20-24 (2000).
69. Wang, X. & Ha, T. Defining single molecular forces required to activate integrin and notch signaling. *Science* **340**, 991-994 (2013).
70. Ruhnow, F., Zwicker, D. & Diez, S. Tracking Single Particles and Elongated Filaments with Nanometer Precision. *Biophys J* **100**, 2820-2828 (2011).
71. Urnavicius, L. *et al.* Cryo-EM shows how dynactin recruits two dyneins for faster movement. *Nature* **554**, 202-206 (2018).

Acknowledgments

We are grateful to the members of the Yildiz laboratory for helpful discussions and carefully reading the manuscript, Andrew P. Carter for providing dynein expression plasmids, and Eva Nogales and Juan P. Bertoldi for mass photometry. This work was funded by grants from the NIH (GM136414), and NSF (MCB-1055017, MCB-1617028) to A.Y.

Author contributions

Y.Z. and A.Y. conceived the study and designed the experiments. Y.Z. prepared the constructs and isolated the proteins. Y.Z. and S.O. labeled the proteins with fluorescent dyes and performed the motility and Co-IP experiments. Y.Z. and A.Y. wrote the manuscript, and all authors read and commented on the manuscript.

Competing Interests Statement

All authors declare no competing interests.

Figures

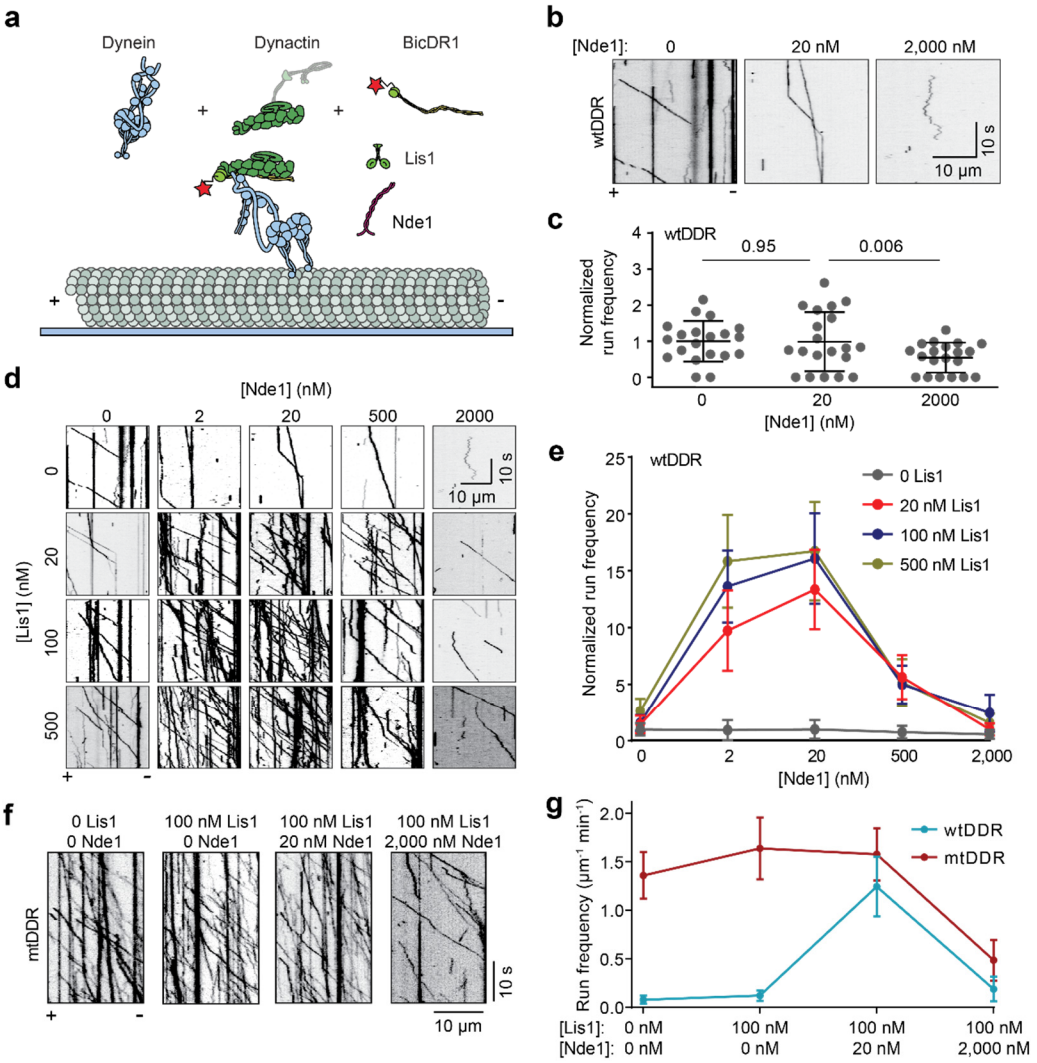

Figure 1. **Nde1 biphasically regulates wtDDR motility together with Lis1. a.** In vitro reconstitution of dynein motility using dynein, dynactin, BicDR1, Lis1, and Nde1 on surface-immobilized microtubules. The red star represents an LD655 dye attached to BicDR1 for TIRF imaging. **b.** Representative kymographs show the motility of wtDDR in the presence of 0, 20 nM, and 2,000 nM Nde1 and the absence of Lis1. **c.** Normalized run frequency distribution of wtDDR under different Nde1 concentrations. The center line and whiskers represent the mean and s.d., respectively (N = 20 microtubules for each condition). P values are calculated from a two-tailed t-test. **d.** Representative kymographs show the motility of wtDDR in the presence of 0 - 500 nM Lis1 and 0 - 2,000 nM Nde1. **e.** The run frequency distribution of wtDDR with different Lis1 and Nde1 concentrations (mean ± s.d.; N = 20 microtubules for each condition). Results were normalized to the 0 nM Lis1 and 0 nM Nde1 condition. **f.** Representative kymographs showing the motility of mtDDR complexes with or without Nde1 and Lis1. **g.** Absolute run frequencies of wtDDR and mtDDR with different Nde1 and Lis1 concentrations (mean ± s.d.; N = 10 for each condition).

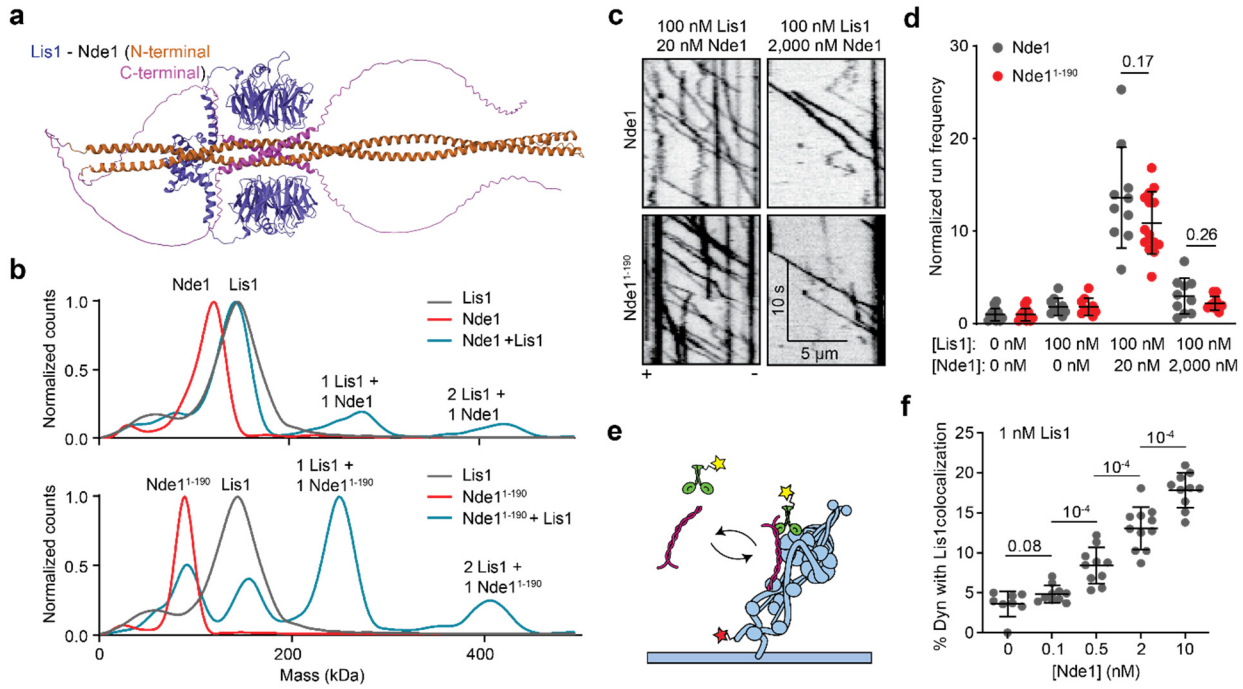

Figure 2. **The N-terminal coiled-coil of Nde1 tethers Lis1 to dynein and drives biphasic regulation. a.** AlphaFold2 prediction of Lis1 (purple) binding to Nde1 (orange: N-terminal, pink: C-terminal). **b.** Mass photometry profiles for Lis1 binding to Nde1 (top) or Nde1$^{1-190}$ (bottom) showing increased binding affinity with Nde1$^{1-190}$. **c.** Representative kymographs show wtDDR motility with Nde1 or Nde1$^{1-190}$. **d.** The run frequency distribution of Nde1 and Nde1$^{1-190}$ under different Lis1 and Nde1 concentrations. Results were normalized to the 0 nM Lis1 and 0 nM Nde1 condition. From left to right, N = 14, 14, 10, 10, 10, 14, 10, and 10 microtubules. **e.** Schematics of single molecule colocalization assay. WT dynein was labeled with both biotin and Alexa488 and immobilized on a glass surface. 1 nM LD555-labeled Lis1 and different concentrations of unlabeled Nde1 were flown into the chamber for observation of Lis1 colocalization to surface-immobilized dynein. **f.** Percent colocalization of surface-immobilized dyneins with LD555-Lis1 under different concentrations of Nde1. From left to right, N = 8, 10, 10, 11, and 10 imaging areas (40 µm x 40 µm) with at least 100 immobilized dynein spots. In **d** and **f**, the center line and whiskers represent the mean and s.d., respectively. P values are calculated from a two-tailed t-test.

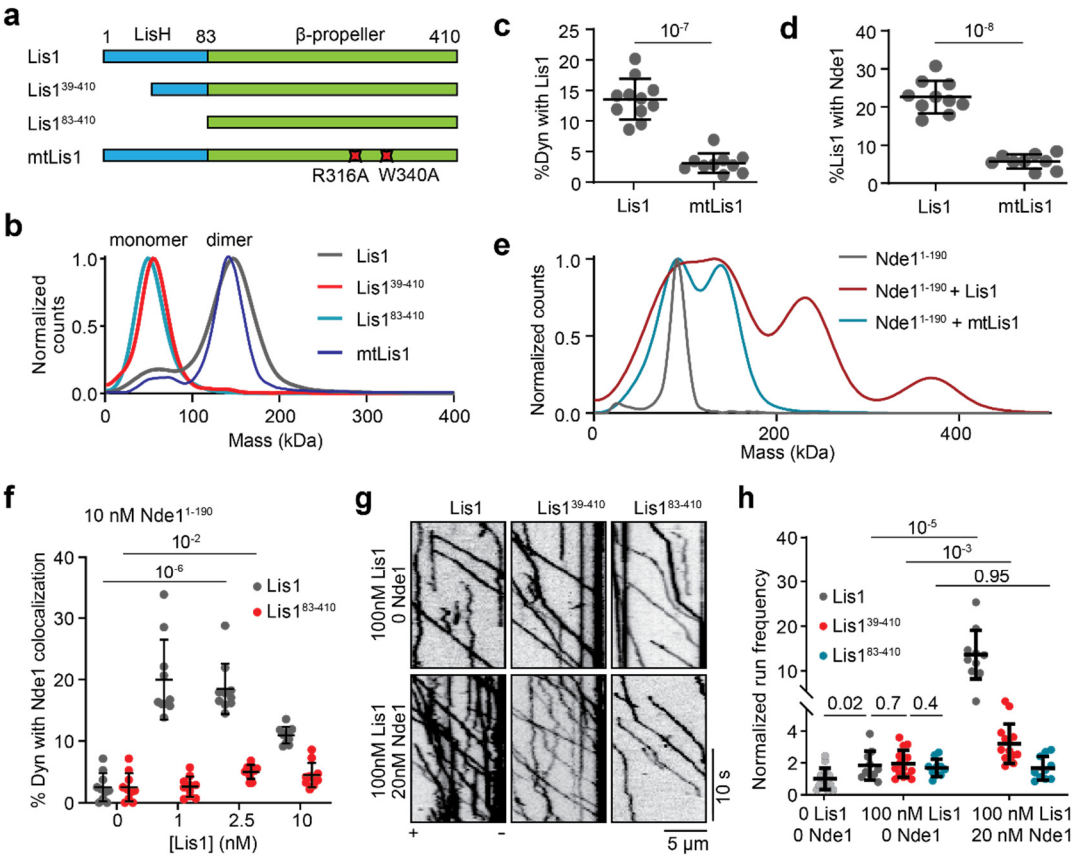

Figure 3. **Nde1 and dynein share the same binding site on Lis1. a.** Schematics of N-terminal truncated Lis1 constructs, and a dynein binding mutant of Lis1 (mtLis1). **b.** Mass photometry shows Lis1 and mtLis1 form a dimer, but Lis1$^{39\text{-}140}$ and Lis1$^{83\text{-}140}$ are monomers. **c.** Percent colocalization of Alexa488-labeled dynein with LD655-labeled 10 nM Lis1 or mtLis1 in solution. From left to right, N = 11 and 10 imaging areas (40 µm x 40 µm) with at least 100 immobilized dynein spots. **d.** Percent colocalization of Alexa488-labeled surface-immobilized Lis1 with LD655-labeled 10 nM Nde1 in solution. From left to right, N = 10 and 9 imaging areas (40 µm x 40 µm) with at least 100 immobilized Lis1 spots. **e.** Mass photometry shows Nde1$^{1\text{-}190}$ forms a complex with Lis1 but does not bind mtLis1. **f.** Percent colocalization of Alexa488-labeled dynein with LD655-labeled Nde1$^{1\text{-}190}$ under increasing concentrations of Lis1 or Lis1$^{83\text{-}410}$ in solution (N = 10 imaging areas (40 µm x 40 µm) with at least 100 immobilized dynein spots for each condition). **g.** Representative kymographs show the motility of wtDDR with 0 - 100 nM Lis1 and 0 - 20 nM Nde1. **h.** The run frequency distribution of wtDDR with 0 -100 nM Lis1 and 0 - 20 nM Nde1. From left to right, N = 14, 10, 15, 10, 10, 14, and 10, respectively. Results were normalized to the 0 nM Lis1 and 0 nM Nde1 condition. In **c, d, f,** and **h**, the center line and whiskers represent the mean and s.d., respectively. P values are calculated from a two-tailed t-test.

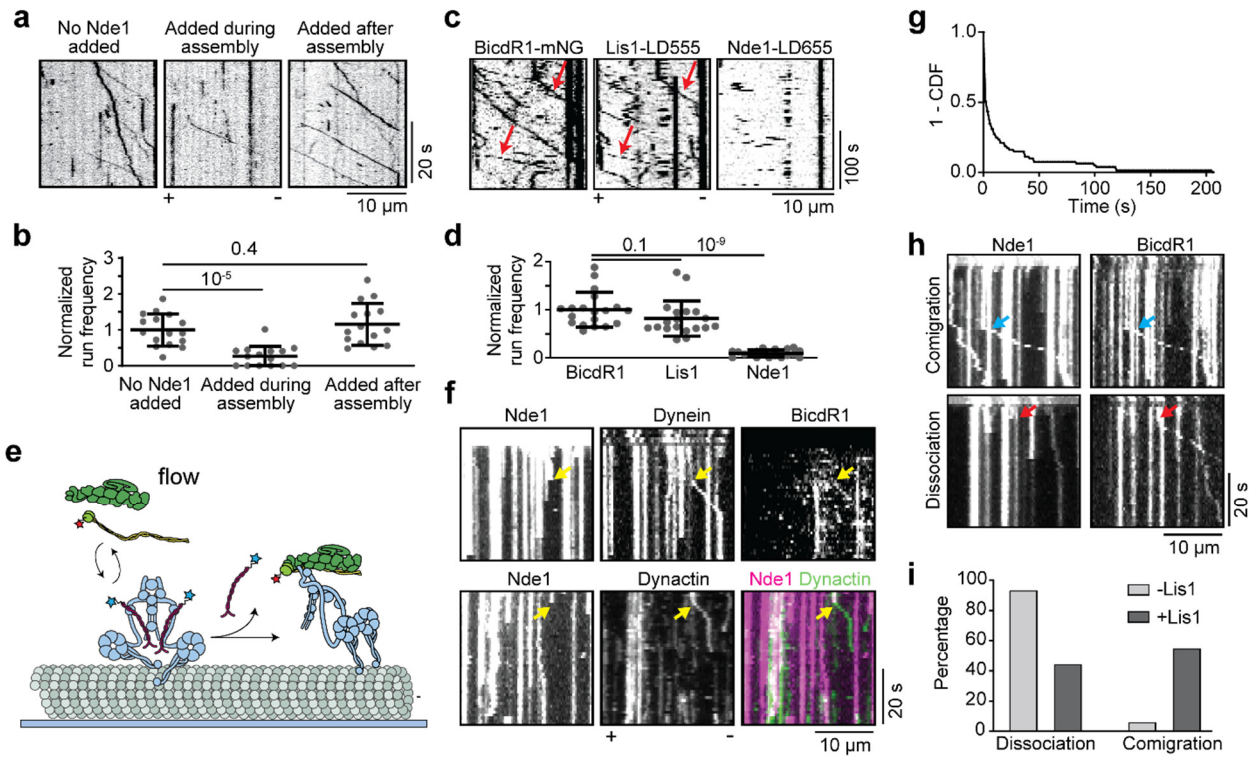

Figure 4. **Nde1-binding is incompatible with DDR assembly and is released before processive motility. a.** Representative kymographs show wtDDR motility with Nde1 added before or after the assembly of the DDR complex. **b.** Normalized run frequency distribution of wtDDR with Nde1 added before or after the assembly. From left to right, N = 16, 15, and 15, respectively; mean values are 1, 0.264, and 1.157, respectively. **c.** Representative kymographs of three-color imaging of BicDR1-mNG, 20 nM LD555-Lis1, and 20 nM LD655-Nde1. Red arrows show the comigration of Lis1 with a processive DDR complex. **d.** Normalized run frequency distribution of BicDR1-mNG, LD555-Lis1, and Nde1-LD655, respectively. N = 19 microtubules for each condition. **e.** Schematics show real-time monitoring of the initiation of wtDDR motility. Microtubules were decorated with WT dynein-GFP and Nde1-LD655 in the absence of Lis1. During imaging, dynactin and BicDR1 were flown into the chamber. Either BicDR1 or dynactin was labeled with LD555. **f.** Example kymographs show Nde1 colocalizes with a component of the DDR complex (dynein, BicDR1, or dynactin) on a microtubule, and the Nde1 signal disappears before the initiation of wtDDR motility. Yellow arrows represent the release of Nde1 followed by the motility of the DDR complex. **g.** The inverse cumulative distribution function (1 - CDF) of time between the disappearance of the colocalized Nde1 signal and the beginning of wtDDR motility. **h.** Representative kymographs show dissociation (red arrows) or comigration (blue arrows) of Nde1 with DDR during the initiation of dynein motility in the presence of Lis1. **i.** Percentage of Nde1 that dissociates from or comigrates with DDR in the presence or absence of Lis1. In **b** and **d**, the center line and whiskers represent the mean and s.d., respectively. P values are calculated from a two-tailed t-test.

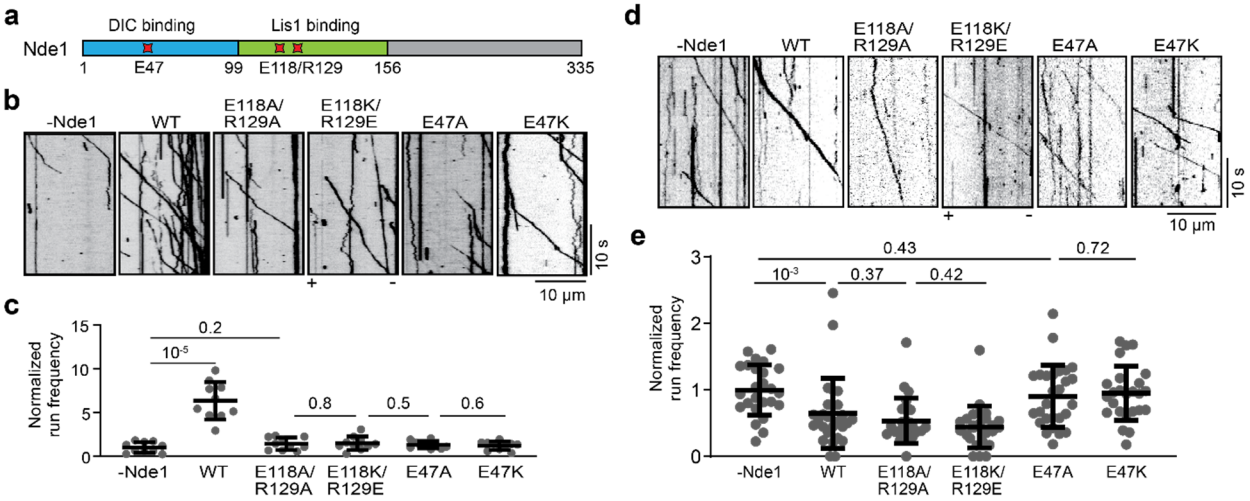

Figure 5. Distinct roles of dynein and Lis1 binding of Nde1 in dynein regulation. a. Schematics show critical residues that facilitate Nde1 binding to Lis1 (E118 and R129) and dynein (E47). **b.** Representative kymographs show wtDDR motility with or without 20 nM WT or mutant Nde1 in the presence of 100nM Lis1. **c.** Normalized run frequency distribution of wtDDR with or without 20 nM WT or mutant Nde1 in the presence of 100nM Lis1. N = 10 microtubules for each condition. **d.** Representative kymographs of mtDDR motility with 500 nM of WT or mutant Nde1 in the absence of Lis1. **e.** Normalized run frequency distribution of mtDDR with or without 500 nM of WT or mutant Nde1 in the absence of Lis1. From left to right, N = 25, 27, 25, 26, 27, and 25 microtubules, respectively. In **c** and **e**, results were normalized to the 100 nM Lis1 and 0 nM Nde1 condition. The center line and whiskers represent the mean and s.d., respectively. P values are calculated from a two-tailed t-test.

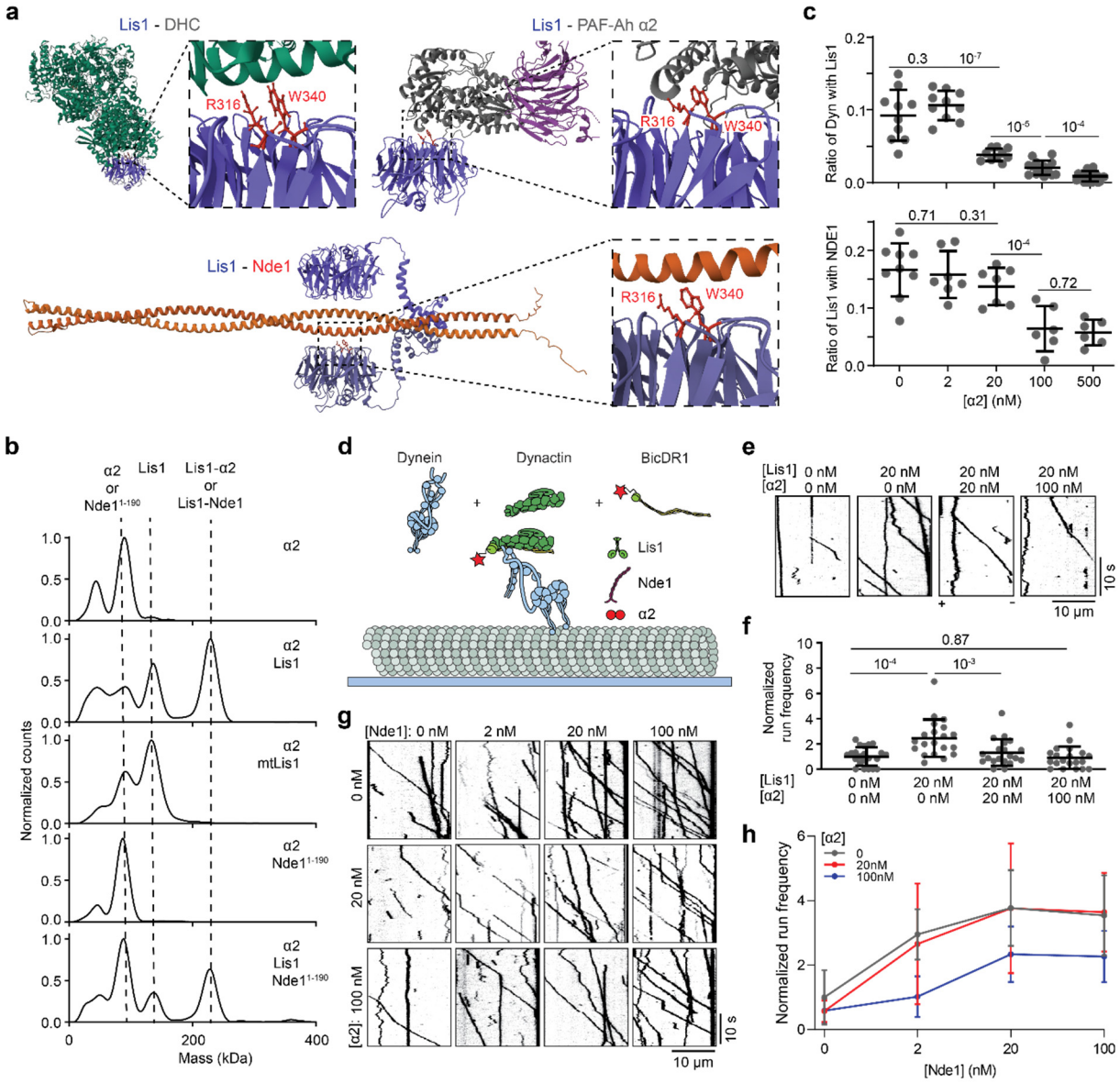

Figure 6. **Nde1 binding rescues Lis1 from its antagonist, α2. a.** Structures of Lis1-DHC (PDB ID: 8DYV[61]), Lis1-α2 (PDB ID: 1VYH[14]), and Lis1-Nde1$^{1-190}$ (predicted by AlphaFold2). Insets show that Lis1 residues (R316 and W340) that facilitate binding to dynein are also critical for Lis1 binding to Nde1 and α2. **b.** Mass photometry reveals that α2 forms a complex with Lis1, but not with mtLis1, and α2 does not form a ternary complex with Lis1 and Nde1$^{1-190}$. **c.** (Top) Ratios of surface-immobilized dynein colocalized with Lis1 in the presence of 2 nM Lis1 and increasing concentrations of α2. (Bottom) Ratios of surface-immobilized Lis1 colocalized with Nde1 in the presence of 50 nM Nde1 and increasing concentrations of α2. From left to right, N = 10, 10, 10, 14, and 19 (Top) and 9, 7, 7, 6, and 6 (Bottom) imaging areas (40 µm x 40 µm) with at least 100 immobilized dyneins (Top) and Lis1 (Bottom) spots. **d.** Schematics of the in vitro wtDDR motility assay in the presence of Lis1, Nde1, and α2. **e.** Representative kymographs show wtDDR motility under 0-100 nM α2 and 0-20 nM Lis1 in the absence of Nde1. **f.** The run frequency distribution of wtDDR under different Nde1 and α2 concentrations. Results were

normalized to the 0 nM Lis1 and 0 nM α2condition. From left to right, N = 22, 20, 20, and 20 microtubules. **g.** Representative kymographs show wtDDR motility under different concentrations of α2 and Nde1 in the presence of 20 nM Lis1. **h.** The run frequency of wtDDR under different concentrations of α2 and Nde1 in the presence of 20 nM Lis1 (mean ± s.d.; N = 20 microtubules for each condition). Results were normalized to the 20 nM Lis1, 0 nM α2, and 0 nM Nde1 condition. In **c** and **f**, the center line and whiskers represent the mean and s.d., respectively. P values are calculated from a two-tailed t-test.

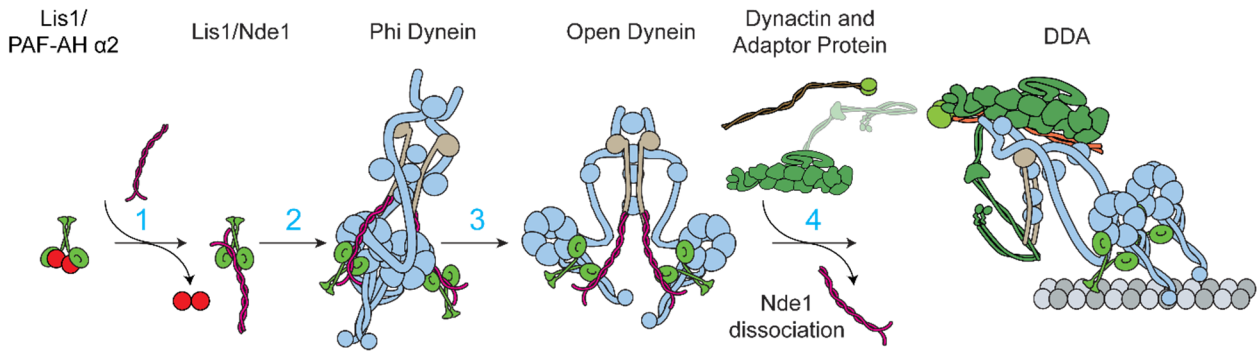

Figure 7. Model for the activation of the dynein transport machinery by Lis1/Nde1. Lis1 is inhibited by its antagonist α2. (1) Nde1 binding to Lis1 releases α2 from Lis1. (2) Dynein forms an autoinhibited phi conformation through self-dimerization of the motor domains. While the Lis1 binding site at the AAA+ ring is inaccessible in the phi conformation, Nde1 binds to DIC and positions Lis1 near its dynein binding site. (3) Transient opening of dynein enables tethered Lis1 to bind the dynein motor domain. Lis1 binding stabilizes the open conformation of dynein because it is sterically incompatible with the phi conformation. (4) Open dynein binds to dynactin and a cargo adaptor and switches to the parallel conformation. Dynactin binding to DIC releases Nde1 from dynein. Subsequently, Lis1 also dissociates from dynein during or after the initiation of processive motility. While binding of two Lis1/Nde1 per dynein has been shown in this model, single Lis1/Nde1 binding may also be sufficient to activate DDA assembly.

Supplementary Information

1. Supplementary Tables

Construct	Vector	Source	Figures
GFP-DYNH1C1-SNAPf-IC2C-LIC2-Robl1-Tctex1-LC8	pOmniBac-pIDC	Carter Lab	F1b-e,g, F2c, d, F3g,h, F4, F5, F6e-h S1, S4b, S5a-c, S6a,b, S7
SNAPf-DYNH1C1-IC2C-LIC2-Robl1-Tctex1-LC8	pOmniBac-pIDC	Schlager et al. 2014 [9]	F2f, F3c,f, F6c, S4a,
SNAPf-DYNH1C1$^{R1567E, K1610E}$-IC2CLIC2-Robl1-Tctex1-LC8	pOmniBac-pIDC	Zhang et al. 2017 [6]	F1f,g, S2, S6c,d
BicDR1-SNAPf	pOmniBac	Urnavicius et al., 2018 [71]	F1, F2c,d, F3g,h, F4f-i, F5, F6e-h, S1, S2, S5b,c, S6, S7
BicDR1-mNeonGreen	pOmniBac	This study	F4a-d
Lis1-SNAPf	pOmniBac	Elshenawy et al., 2020 [16]	F1d-g, F2, F3, F4c,d,h,i, F5b,c, F6, S1, S2, S4, S5, S7
Lis1$^{39-410}$-SNAPf	pOmniBac	This study	F3b,g-h, S5d
Lis1$^{83-410}$-SNAPf	pOmniBac	This study	F3b,f-h, S5d
Lis1$^{R316A, W340A}$-SNAPf	pOmniBac	This study	F3b-e, S5a-c
Nde1-SNAPf	pOmniBac	This study	F1, F2, F3d,g,h, F4, F6c,e-h, S1, S2, S3, S4, S5b,c, S7
Nde1$^{1-190}$-SNAPf	pOmniBac	This study	F2b-d, F3e,f, F6b, S3
Ybbr-Nde1	pOmniBac	This study	F5
Ybbr-Nde1$^{E118A, R129A}$	pOmniBac	This study	F5
Ybbr-Nde1$^{E118K, R129E}$	pOmniBac	This study	F5
Ybbr-Nde1^{E47A}	pOmniBac	This study	F5
Ybbr-Nde1^{E47K}	pOmniBac	This study	F5
PAFAH α2-SNAPf	pOmniBac	This study	F6, S6, S7

Supplementary Table 1. The list of constructs used in this study. Dynein chains were codon-optimized for *Spodoptera frugiperda* (SF9) expression and inserted into the pOmniBac backbone. Plasmid containing Nde1 was obtained from Origene. Nde1, Lis1, PAF-AH α2, and BicDR1 constructs were cloned into the pOmniBac backbone. Each construct was tagged with an N-terminal 6xHis-ZZ-TEV site for affinity purification and Tev protease cleavage during protein purification (F: Figure, S: Supplementary Figure).

2. Supplementary Figures

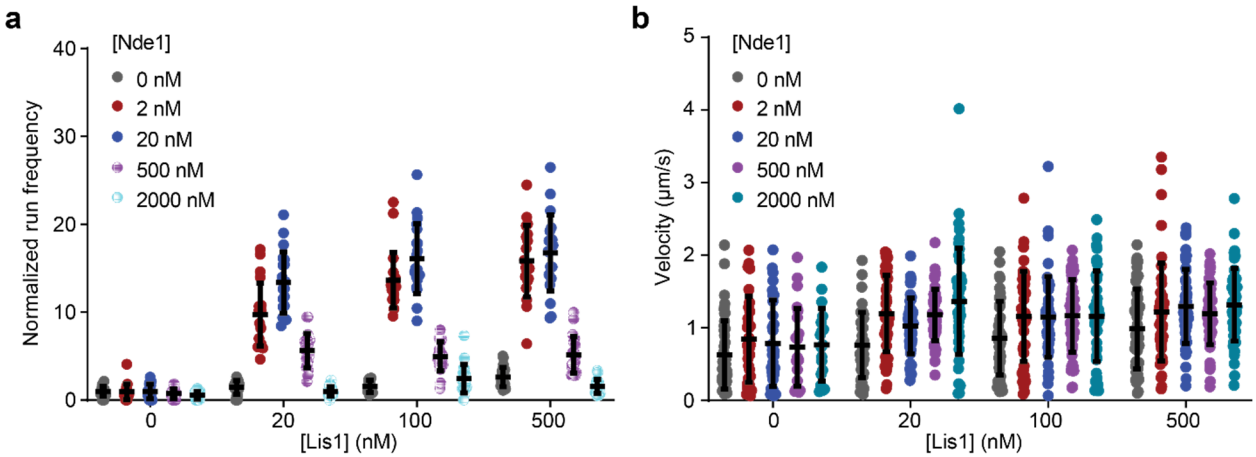

Supplementary Figure 1. Run frequency and velocity of wtDDR under different Lis1 and Nde1 concentrations. a. Normalized run frequency distribution of wtDDR under different Lis1 and Nde1 concentrations. Results were normalized to the 0 nM Lis1 and 0 nM Nde1 condition. The center line and whiskers represent the mean and s.d., respectively. N = 20 microtubules for each condition. **b.** Velocity distribution of wtDDR under different Lis1 and Nde1 concentrations. The center line and whiskers represent the mean and s.d., respectively. N = 50 processive DDR complexes for each condition.

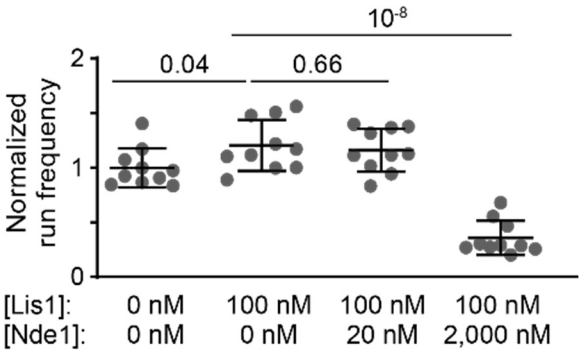

Supplementary Figure 2. mtDDR motility is inhibited by excess Nde1. Normalized run frequencies distribution of mtDDR under different Lis1 and Nde1 concentrations. The center line and whiskers represent the mean and s.d., respectively (N = 10 microtubules for each condition).

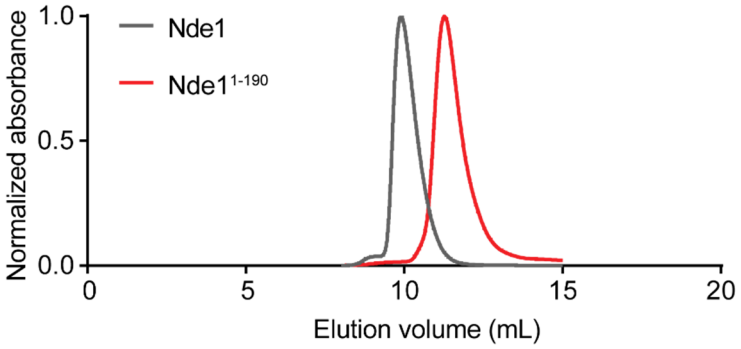

Supplementary Figure 3. Elution profiles of Nde1 and Nde1$^{1-190}$ from a size exclusion column.

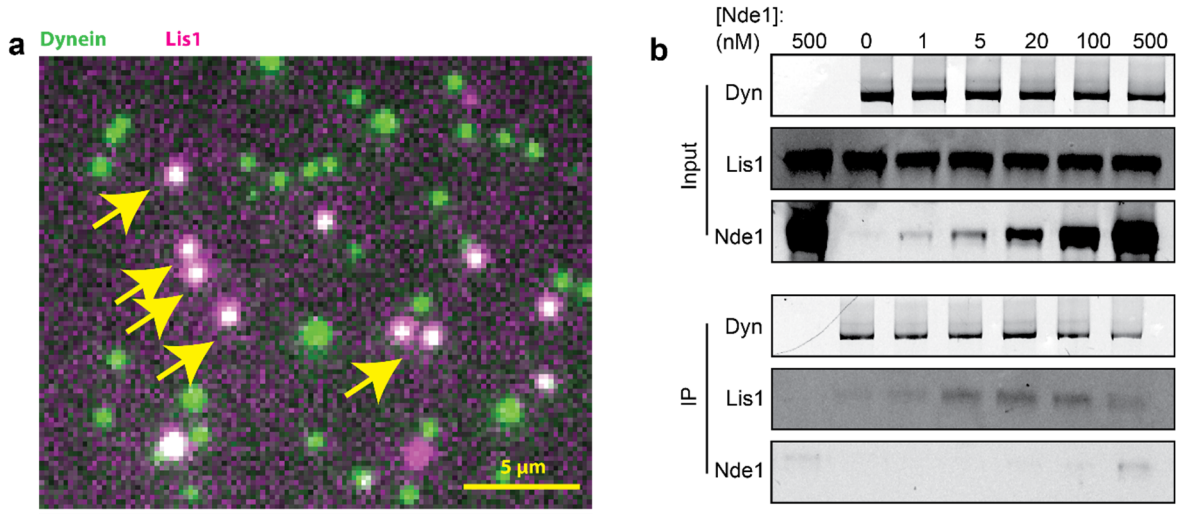

Supplementary Figure 4. Nde1 increases Lis1 association with dynein. a. Representative overlay imaging of surface-immobilized and Alexa488-labeled dynein and Lis1-LD555. Arrows show examples of colocalization between dynein and Lis1. **b.** Co-immunoprecipitation (Co-IP) of Lis1 pulled down by dynein-GFP with increasing Nde1 concentrations.

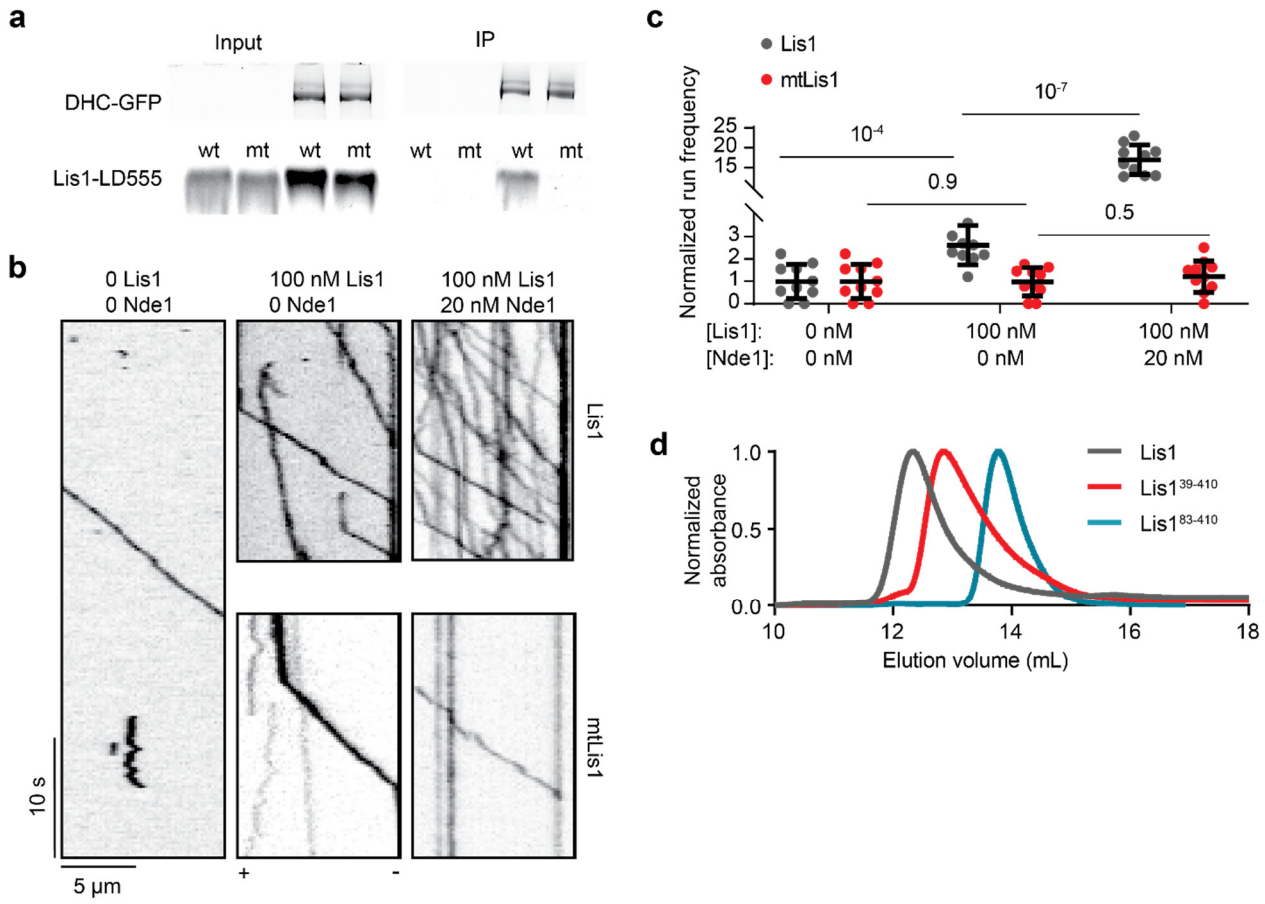

Supplementary Figure 5. Dynein binding mutant of Lis1 does not stimulate dynein activation with or without Nde1. a. Co-IP of Lis1 or mtLis1 with WT dynein-GFP using anti-GFP beads. **b.** Representative kymographs show wtDDR motility with 100 nM Lis1 or mtLis1 with or without 20 nM Nde1. **c.** The run frequency distribution of wtDDR complexes with 100 nM Lis1 or mtLis1 with or without 20 nM Nde1. Results were normalized to the 0 nM Lis1 and 0 nM Nde1 condition. The center line and whiskers represent the mean and s.d., respectively. N = 10 microtubules for each condition. P values are calculated from a two-tailed t-test. **d**. Elution profiles of Lis1, Lis1$^{39-410,}$ and Lis1$^{83-410}$ from a size exclusion column.

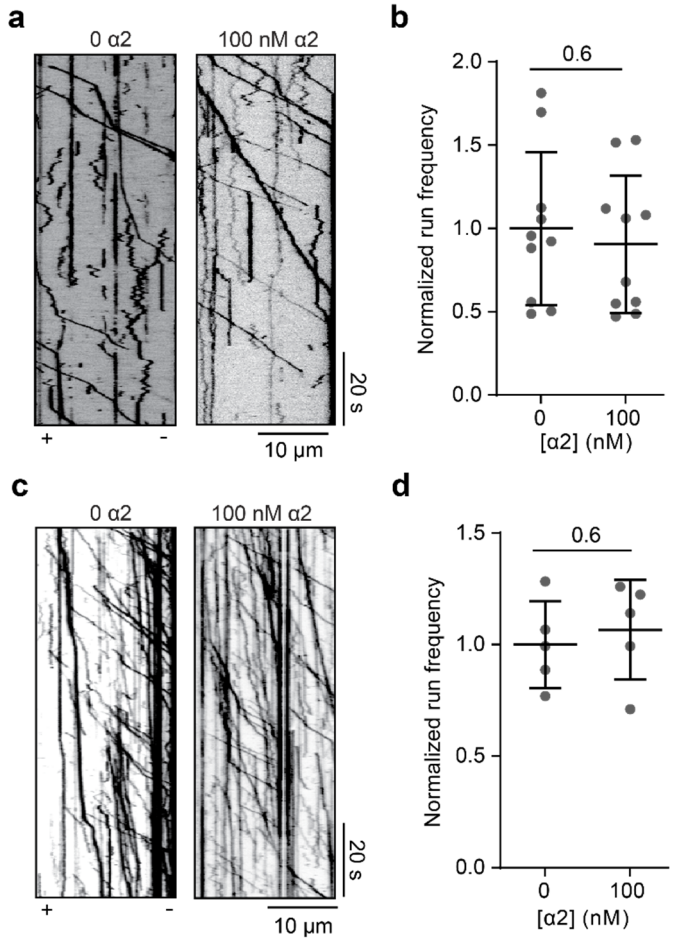

Supplementary Figure 6. α2 does not directly influence DDR motility. a. Representative kymographs show wtDDR motility with or without 100 nM α2. **b.** The run frequency distribution of wtDDR with or without 100 nM α2, respectively. Results were normalized to the 0 nM α2 condition. N = 10 microtubules for each condition. **c.** Representative kymographs of the motility of mtDDR complexes with or without α2. **d.** The run frequency distribution of mtDDR with or without 100 nM α2. Results were normalized to the 0 nM α2 condition. N = 5 microtubules for each condition. In **b** and **d**, the center line and whiskers represent the mean and s.d., respectively. P values are calculated from a two-tailed t-test.

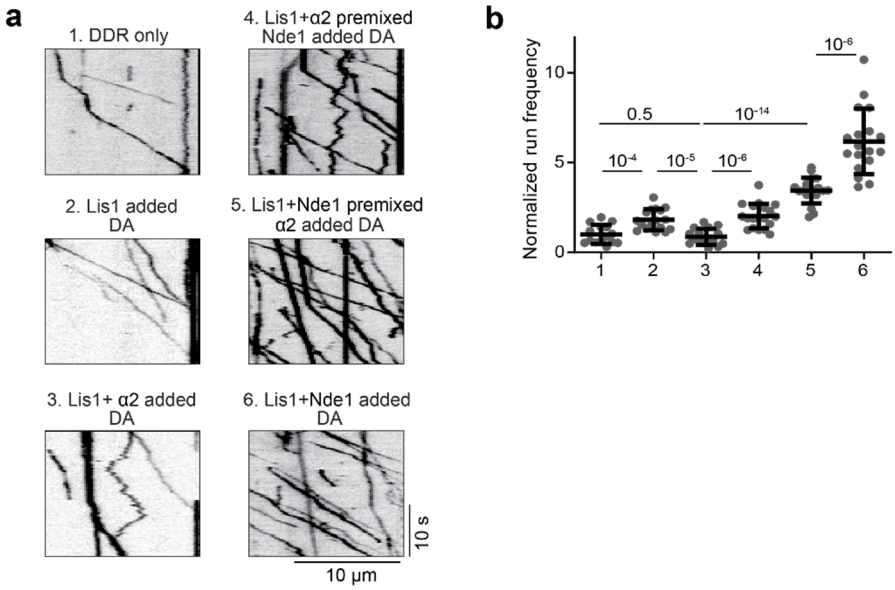

Supplementary Figure 7. Nde1 prevents Lis1 inhibition and enhances wtDDR motility in the presence of α2. a. Representative kymographs showing the motility of wtDDR complexes under different wtDDR assembly conditions. The assays were performed in 10 nM WT dynein, 100 nM BicDR1, 150 nM dynactin, 20 nM Lis1, 100 nM Nde1, and 100 nM α2 (DA: during assembly). **b**. The run frequency distribution of wtDDR under different complex assembly conditions shown in a. Results were normalized to the 0 nM α2, 0 nM Lis1, and 0 nM Nde1 condition. From left to right, N = 15, 17, 16, 19, 19, and 18 microtubules. The center line and whiskers represent the mean and s.d., respectively. P values are calculated from a two-tailed t-test.

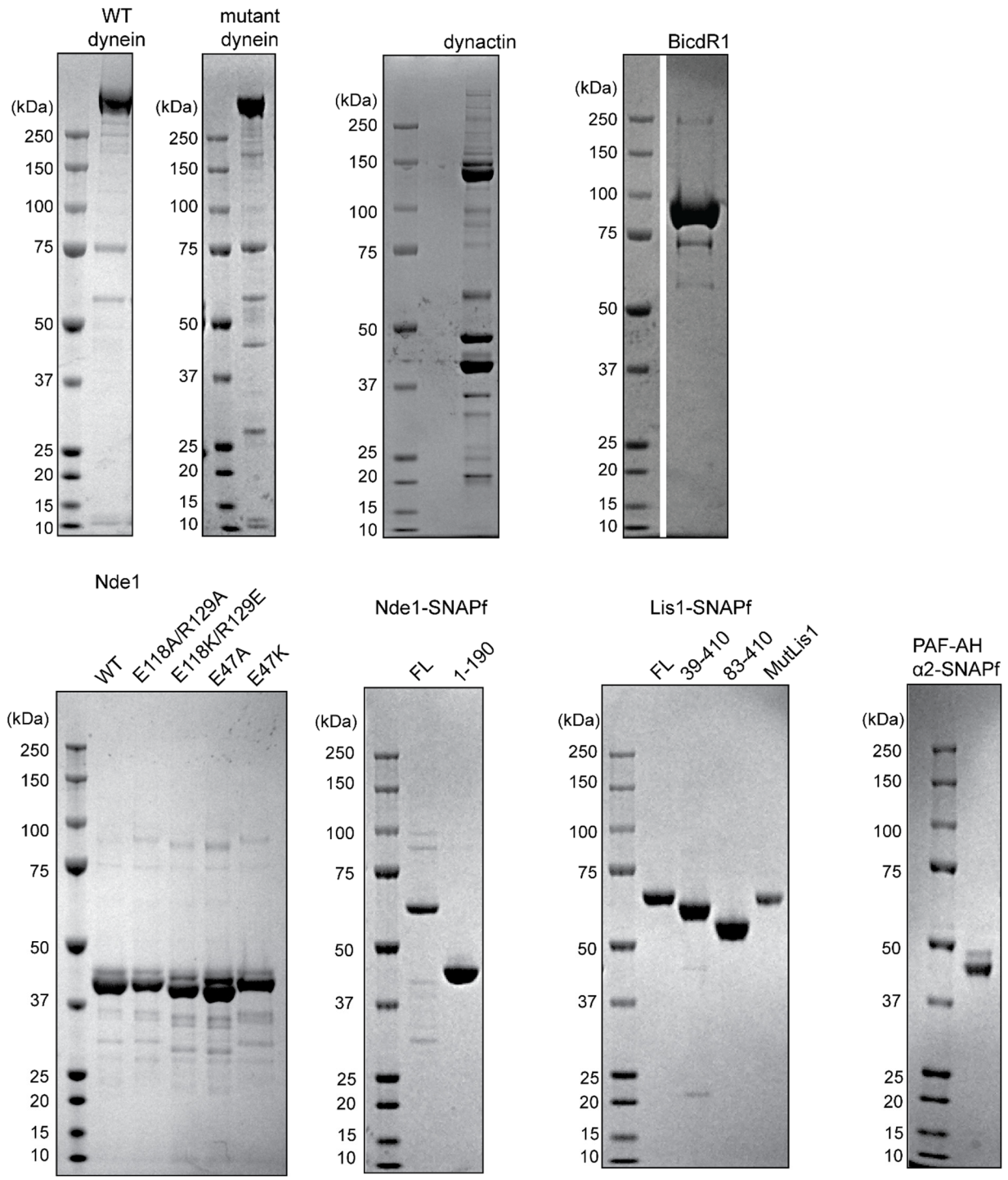

Supplementary Figure 8. Denaturing gel pictures of purified proteins in this study.

3. Supplementary Movie Legends

Supplementary Movie 1. wtDDR motility is enhanced by Lis1 and Nde1. Single molecule motility recording of wtDDR complexes in the presence of 0-100nM Lis1 and 0- 2,000 nM Nde1 using a TIRFM assay. The fluorescence signal corresponds to BicDR1-mNeonGreen, while other subunits and factors are unlabeled. Related to Figure 1d.

Supplementary Movie 2. Nde1 does not substantially affect the run frequency of mtDDR. Single molecule motility recording of mtDDR complexes with or without added Lis1 or Nde1 using a TIRFM assay. The fluorescence signal corresponds to BicDR1-mNeonGreen, while other subunits and factors are unlabeled. Related to Figure 1f.

Supplementary Movie 3. AlphaFold2 prediction of Lis1 (purple) binding to Nde1. Related to Figure 2a.

Supplementary Movie 4. wtDDR motility is not enhanced by Nde1 mutants that do not bind either dynein or Lis1. Single molecule motility recording of wtDDR complexes with 100 nM Lis1 and 20 nm Nde1 or different Nde1 mutants using a TIRFM assay. The fluorescence signal corresponds to BicDR1-mNeonGreen, while other subunits and factors are unlabeled. Related to Figure 5b.